Author Manuscript

Author Manuscript

Author Manuscript

Author Manuscript

HHS Public Access

Author manuscript

Curr Biol. Author manuscript; available in PMC 2022 July 26.

Published in final edited form as:

Curr Biol. 2021 July 26; 31(14): 3028–3039.e7. doi:10.1016/j.cub.2021.04.062.

Vmp1, Vps13D and Marf/Mfn2 function in a conserved pathway to regulate mitochondria and ER contact in development and disease

James L. Shen[1], **Tina M. Fortier**[1], **Yan G. Zhao**[1], **Ruoxi Wang**[1], **Margit Burmeister**[2], **Eric H. Baehrecke**[1,3,4]

[1]Department of Molecular, Cell and Cancer Biology, University of Massachusetts Medical School, Worcester, MA 01605 USA

[2]Michigan Neuroscience Institute and Dept of Computational Medicine & Bioinformatics, University of Michigan, Ann Arbor, MI 48109, USA

[3]Lead Contact

[4]Twitter: @BaehreckeLab

SUMMARY

Mutations in *Vps13D* cause defects in autophagy, clearance of mitochondria and human movement disorders. Here we discover that Vps13D functions in a pathway downstream of Vmp1 and upstream of Marf/Mfn2. Like *vps13d, vmp1* mutant cells exhibit defects in autophagy, mitochondrial size and clearance. Through the relationship between *vmp1* and *vps13d*, we reveal a novel role for Vps13D in the regulation of mitochondria and endoplasmic reticulum (ER) contact. Significantly, the function of Vps13D in mitochondria and ER contact is conserved between fly and human cells, including fibroblasts derived from patients suffering from *VPS13D* mutation-associated neurological symptoms. *vps13d* mutants have increased levels of Marf/MFN2, a regulator of mitochondrial fusion. Importantly, loss of *marf/MFN2* suppresses *vps13d* mutant phenotypes, including mitochondria and ER contact. These findings indicate that Vps13d functions at a regulatory point between mitochondria and ER contact, mitochondrial fusion and autophagy, and help to explain how Vps13D contributes to disease.

Graphical Abstract

*Correspondence to: Eric H. Baehrecke, Department of Molecular, Cell, and Cancer Biology, 423 Lazare Research Building, 364 Plantation St., University of Massachusetts Medical School, Worcester, MA 01605, USA. Tel:+1-508-856-6733, eric.baehrecke@umassmed.edu.

Author contributions

J.L.S., Y.G.Z. and E.H.B. designed experiments, J.L.S. and T.M.F. performed experiments, R.W. and M.B. provided resources, J.L.S. and E.H.B. wrote the manuscript and all authors commented on it.

Declaration of Interests

EHB is a member of the Advisory Board of Current Biology. All other authors declare no competing interests.

Publisher's Disclaimer: This is a PDF file of an unedited manuscript that has been accepted for publication. As a service to our customers we are providing this early version of the manuscript. The manuscript will undergo copyediting, typesetting, and review of the resulting proof before it is published in its final form. Please note that during the production process errors may be discovered which could affect the content, and all legal disclaimers that apply to the journal pertain.

Author Manuscript Author Manuscript Author Manuscript Author Manuscript

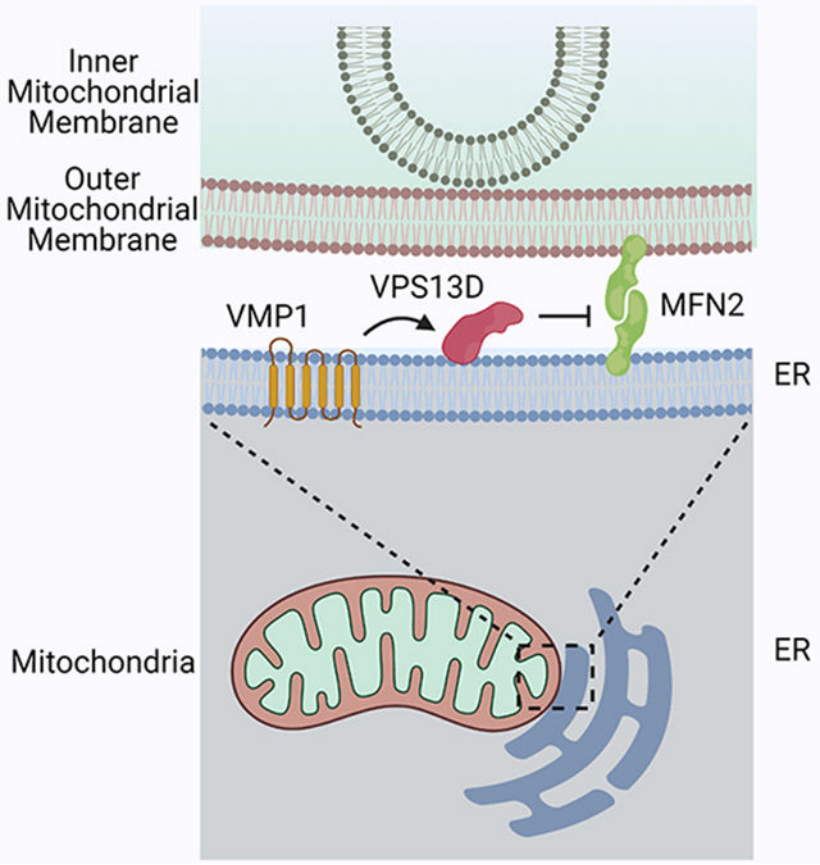

eTOC blurb

The clearance of mitochondria by mitophagy is important for cell health. Shen *et al.* identify Vps13D as functioning in a pathway with Vmp1 and Marf/Mfn2 to regulate mitophagy. Loss of *Vps13D* in flies and cells derived from patients with movement disorders also impacts mitochondria and ER contact, and these cellular defects depend on Marf/MFN2.

Keywords

Vps13D; Vmp1; autophagy; mitochondria; *Drosophila*; membrane contact

INTRODUCTION

Autophagy, the lysosome-dependent clearance of intracellular contents, plays important roles in organism development and health. The failure to remove mitochondria by autophagy, or mitophagy, results in defects in cellular homeostasis and health, and contributes to multiple diseases.[1] For example, mutations in genes responsible for mitophagy manifest as inheritable forms of Parkinson's disease and Alzheimer's disease.[2] As a result, it is becoming clear that understanding the mechanisms that regulate mitophagy under different cellular contexts is crucial to our understanding of biology and health.

Author Manuscript Author Manuscript Author Manuscript Author Manuscript

The mechanisms underlying mitophagy in animals have been defined through studies of derived cell lines. These elegant studies of PINK1- and Parkin-dependent mitophagy have significantly advanced our understanding of this important process. Importantly, these studies have focused on mitophagy in response to mitochondrial damage, where cells are treated with mitochondrial depolarizing agents that are not typically seen in a physiological setting.[3] Mitophagy in animals can occur in response to other stimuli, suggesting mitophagy in cells and tissues under physiological conditions do not always utilize the same regulatory pathways.[4,5] During *Drosophila* development, the larval intestine undergoes an autophagy driven remodeling process where cells reduce in size and mitochondria are cleared by mitophagy.[6, 7] Mitophagy is driven by the steroid hormone ecdysone, and occurs without the need to induce mitochondrial damage through incubation with uncoupling reagents.[8, 9] This system allowed us to identify *vps13d* and other genes as regulators of autophagy under physiological conditions.[6,7] Importantly, *vps13d* is an essential and conserved gene that regulates mitochondrial clearance, mitochondrial morphology, and has been implicated in human movement disorders.[7, 10, 11]

Vacuolar protein sorting 13 (*vps13*) was discovered in yeast, and animals possess four evolutionarily conserved Vps13 family members *Vps13A-D*.[12,13] Yeast VPS13, as well as mammalian Vps13A and C, have been implicated in the regulation of inter-organelle contact and lipid transport.[14,15] However, these studies fail to address if loss-of-function mutants of these human paralogs repress or enhance membrane contacts. Furthermore, no study has linked VPS13D specifically to regulation of membrane contacts.

Members of the Vps13 family possess unique functional requirements. In contrast to *VPS13A-C, VPS13D* is one of the most vital genes for survival in human cell lines,[16,17] and is essential for *Drosophila* development.[7] Vps13D is the only Vps13 family member that contains a ubiquitin binding domain, which is required for proper mitochondrial clearance. Furthermore, loss of this ubiquitin binding domain results in enlarged mitochondria. This phenotype is unique in that most autophagy genes required for mitochondrial clearance do not affect mitochondrial size. For example, loss of the autophagy receptor Ref2p/P62 does not result in enlarged mitochondria.[7] Vps13D is also the only Vps13 family member in flies that is required for autophagy.[7] Significantly, mutations in *VPS13D* have been associated with multiple diseases, including altered septic shock mortality and a unique group of familial neurological movement disorders involving ataxia, chorea and dystonia.[10,11,18-20] Despite these findings, it remains unclear how VPS13D regulates autophagy, mitochondrial morphology and contributes to human diseases.

Here we investigate the relationship between *vps13d* and genes that regulate autophagy and mitochondrial morphology. We discover that Vps13D acts downstream of Vmp1/EPG-3, a regulator of autophagy and mitochondria and endoplasmic reticulum (ER) contact. Like Vps13D, loss of Vmp1 disrupts autophagy and mitochondrial morphology. Through this relationship, we identify a novel role for Vps13D as a regulator of mitochondria and ER contact in *Drosophila* and human cell lines, including fibroblasts derived from patients symptomatic for *VPS13D* associated neurodegenerative disease. Importantly, we also discover that Vps13D interacts with the regulator of mitochondrial fusion Marf (Mitofusins in mammals), and that loss of either *marf* in flies or *MFN2* in patient-derived cell lines

Author Manuscript Author Manuscript Author Manuscript Author Manuscript

suppresses *vps13d* mutant phenotypes. Our findings establish Vmp1, Vps13D and Marf/MFN2 as important factors in a pathway that regulates inter-organelle contacts in autophagy and mitochondrial morphology, and help explain the role of *vps13d* in disease.

RESULTS

Vmp1 regulates autophagy, mitophagy and mitochondrial morphology

The essentiality (Figure S1A) and unique role of Vps13D in autophagy among Vps13 family members prompted us to consider if other factors implicated in both autophagy and inter-organelle contact may possess phenotypes that are similar to *vps13d*. Vmp1 (EPG-3 in *C. elegans*) is a conserved regulator of autophagy in worms and mammals, and also influences inter-organelle contacts.[21,22] To test if *Drosophila* Vmp1 (also known as Tango5) has a similar function to Vps13D, we analyzed the function of *vmp1* in larval intestine cells where *vps13d* functions in autophagy, cell size reduction, mitochondrial clearance and maintenance of mitochondrial size. Like *vps13d* mutant cells,[7] cells with reduced Vmp1 function that express *vmp1* RNAi and green fluorescent protein (GFP) did not accumulate mCherryAtg8a autophagy reporter puncta and were unable to reduce in size, unlike neighboring GFP-negative control cells (Figure 1A and B). This was the same phenotype seen in *vps13d* RNAi-expressing and loss of function intestine cells.[7] Similar results were obtained using a distinct RNAi targeting a different *vmp1* sequence (Figure S1B and C).

We next used CRISPR/CAS9 gene editing to create a loss-of-function *vmp1* mutant *Drosophila* named *vmp1(Δ)* (Figure S1D). Homozygous *vmp1(Δ)* mutant animals die during development with a small number of animals surviving until the 3rd instar larval stage. Importantly, an X chromosome duplication containing the *vmp1* open reading frame complemented the *vmp1(Δ)* lethal phenotype (Figure S1E).

We analyzed *vmp1(Δ)* mutant cells for phenotypes that are similar to homozygous *vps13d* mutant intestine cells. Consistent with *vmp1* RNAi knockdown, intestines with homozygous *vmp1(Δ)* mutant cells lacking red fluorescent protein (RFP) accumulated the autophagic cargo receptor Ref2p (p62 in mammals) compared to neighboring control cells that possess RFP (Figure 1C and D), indicating that autophagy is impaired. Similar to homozygous *vmp1(Δ)* mutant cells, Ref2p accumulated in *vps13d (MiMic)* mutant cells (Figure S1F and G).

Mitochondria are cleared by autophagy during intestine development.[6] Therefore, we investigated if Vmp1, like Vps13D, is required for clearance of mitochondria in the intestine. Significantly, homozygous *vmp1(Δ)* mutant intestine cells lacking RFP were unable to clear mitochondria compared to neighboring control cells that express RFP based on persistence of the mitochondrial protein ATP5a (Figure 1E and F). Combined, these data indicate that Vmp1 has similar functions to Vps13D, including the regulation of autophagy and clearance of mitochondria.

We next investigated if the presence of mitochondria in homozygous *vmp1(Δ)* mutant intestine cells was due to a defect in mitophagy. We used the mito-QC system which utilizes a mitochondrial protein tagged with GFP and RFP to detect when mitochondria are

Author Manuscript Author Manuscript Author Manuscript Author Manuscript

delivered to autolysosomes.[4,5] Control intestines that expressed control *luc* RNAi throughout the intestine cleared most mitochondria by 2 hours after pupariation as shown by the presence of RFP-positive and GFP-negative puncta (Figure 2A and B). By contrast, intestines that expressed *vps13d* RNAi or expressed either of two distinct *vmp1* RNAi constructs retained mitochondria that were both RFP- and GFP-positive 2 hours after pupariation (Figure 2A and B). In addition, transmission electron microscopy (TEM) analyses revealed enlarged mitochondria in *vmp1* RNAi-expressing intestine cells compared to control intestine cells at 2 hours after pupariation (Figure 2C and D). Larger mitochondria were also observed by TEM analyses of intestine cells expressing a different *vmp1* RNAi (Figure S2). These data indicate that Vmp1 and Vps13D have similar functions in regulating autophagy, mitophagy and mitochondrial morphology in *Drosophila* intestines.

Vps13D regulates mitochondria and endoplasmic reticulum contact

Vmp1 is a repressor of membrane contact, and the failure to disassemble mitochondria and endoplasmic reticulum (ER) contact alters mitochondrial morphology in *vmp1* mutant mammalian and *C. elegans* cells.[22] We investigated if Vmp1 influences mitochondria and ER contact in *Drosophila* through TEM analyses of intestines 2 hours after pupariation. Intestines with decreased Vmp1 function that express *vmp1* RNAi possessed increased contact between mitochondria and ER compared to *luciferase (luc)* RNAi control cells (Figure 3A and B). The majority of these contact sites were between mitochondria and rough ER. Similar results were obtained with a different *vmp1* RNAi line (Figure S3). These results indicate that Vmp1 regulates mitochondria and ER contact in *Drosophila.*

Given the role of Vmp1 in mitochondria and ER contact, as well as the similarities between *vmp1* and *vps13d* mutant cell phenotypes, we investigated if *vps13d* functions in mitochondria and ER contact by TEM analyses. Intestine cells of either homozygous *vps13d (ΔUBA)*, a mutant lacking the ubiquitin binding domain, or *vps13d(ΔUBA)*/chromosome deficiency (*Df*) for the *vps13d* genomic region had significantly increased mitochondria and ER contact compared to heterozygous *vps13d (ΔUBA)*/wild type control cells 2 hours after pupariation (Figure 3C and D). Like *vmp1* depleted cells, the majority of the ER in contact with mitochondria in *Vps13d* mutant cells were rough ER.

The function of Vps13D in the regulation of mitochondria and ER contact in *Drosophila* prompted us to consider if this phenotype is conserved in humans. Therefore, we analyzed HeLa cells that either lack the ubiquitin binding domain, *VPS13D(ΔUBA)*, or are thought to be a strong loss-of-function mutant, *VPS13D(KO)*. Significantly, we found that mitochondria and ER contact were increased in both *VPS13D* mutant human HeLa cell lines (Figure 3E and F). These results indicate that both *vmp1* and *vps13d* regulate mitochondria and ER contact in *Drosophila* and human cells.

Mutations in *VPS13D* have been associated with familial neurological movement disorders, including ataxia, dystonia, and chorea.[10, 11] Given the conserved function of VPS13D in inter-organelle contact between fly and human HeLa cells, we investigated if patient-derived cells with *VPS13D* mutations have altered mitochondria and ER contact by TEM. Remarkably, mitochondria in fibroblasts that were derived from the symptomatic *VPS13D* mutant (G1190D/Q1106*) patient had increased mitochondria and ER contact compared to

Author Manuscript Author Manuscript Author Manuscript Author Manuscript

the mitochondria in fibroblasts derived from a relative (G1190D/+) and unrelated control (Figure 4A and B).[10] In addition, we analyzed mitochondria and ER contact in a second set of fibroblasts derived from an unrelated family with symptoms associated with the *VPS13D* mutations.[8] Mitochondria from the symptomatic *VPS13D* mutant patient from this family (A4210V/Y1803*) also exhibited increased mitochondria and ER contact compared to mitochondria in fibroblasts derived from both an asymptomatic relative (A4210V/+) and a separate unrelated control (Figure 4C and D). A poor correlation exists between the perimeter of mitochondria in *Vps13d* mutant intestine cells ($R^2 = 0.1456$), HeLa cells ($R^2 = 0.00554$), and patient fibroblasts ($R^2 = 0.00037$) (Figure S4), suggesting that the increase in mitochondria and ER contact in *Vps13d* mutants was not simply due to increased mitochondrial perimeter. Therefore, VPS13D regulates mitochondria and ER contact, this function is conserved from flies to humans, and this phenotype likely contributes to cell health and neurological disease.

Vps13D functions downstream of Vmp1 to regulate mitochondrial morphology and mitophagy

The similarities between *vmp1* and *vps13d* mutant phenotypes suggests that these genes may be in the same genetic pathway regulating mitophagy and mitochondrial size. We analyzed Vps13D protein localization in control and homozygous *vmp1(Δ)* mutant intestine cells 2 hours after pupariation, and found that Vps13D protein puncta were significantly decreased in *vmp1* mutant cells compared to neighboring control cells (Figure 5A and B). These results indicate that Vps13D puncta are dependent on Vmp1. We next investigated if Vps13d influences Vmp1. Antibodies do not exist to detect Vmp1 in *Drosophila*. Therefore, CRISPR/CAS9 was used to tag Vmp1 with GFP on the N terminus (GFP-Vmp1) (Figure S5A). These flies are viable, fertile and complemented the lethal phenotype associated with the *vmp1(Δ)* mutant. GFP-Vmp1 co-localizes with the ER markers Sec61β and SERCA in intestine cells (Figure S5B). In addition, *vmp1* RNAi expression in the entire GFP-Vmp1 larval intestine resulted in retention of mitochondria and increased cell size compared to controls. *vmp1* RNAi throughout the intestine also caused an almost complete ablation of GFP signal, verifying that the GFP puncta were indeed GFP-Vmp1 (Figure S5C). Interestingly, *vps13d(MiMic)* loss-of-function mutant cells did not possess altered GFP-Vmp1 localization (Figure 5C and D), indicating that Vmp1 localization is not dependent on *vps13d* function. Combined, these results suggest that Vps13d functions downstream of Vmp1.

We investigated the relationship between Vmp1 and Vps13d in the clearance of mitochondria. We compared mitochondrial clearance in *vmp1(Δ)* and *vps13d(ΔUBA)* double mutant intestine cells with *vmp1(Δ)*/+ and *vps13d(ΔUBA)* single mutant control cells 2 hours after pupariation. Double mutant cells had similar amounts of mitochondrial ATP5a protein compared to neighboring control cells (Figure 5E and F), suggesting that these genes function in the same pathway to clear mitochondria. Consistent with these findings, loss of *vps13d* function failed to enhance the mitochondrial clearance phenotype caused by expression of *vmp1* RNAi throughout the intestine (Figure S5D).

Author Manuscript Author Manuscript Author Manuscript Author Manuscript

We next used mito-QC to investigate if Vmp1 and Vps13D function in a shared mitophagy pathway. Control intestines that were heterozygous for the *vps13d (ΔUBA)* mutation cleared most mitochondria by 2 hours after pupariation as shown by the presence of RFP-positive and GFP-negative puncta. By contrast, intestines that were homozygous for the *vps13d (ΔUBA)* mutation retained mitochondria that were both RFP- and GFP-positive 2 hours after pupariation (Figure 5G and H). Combined knockdown of *vmp1* by RNAi in a homozygous *vps13d (ΔUBA)* mutant background failed to enhance the *vps13d* mutant mito-QC phenotype (Figure 5G and H), further indicating that *vmp1* and *vps13d* function in the same mitophagy pathway.

To investigate if Vps13D and Vmp1 function in the same pathway to regulate mitochondria and ER contact, we analyzed *vps13d (ΔUBA)/DF* expressing either *vmp1* or control *rfp* RNAi by TEM. Importantly, the combined reduction of both *vmp1* and *vps13d* function failed to enhance either the increased mitochondrial size or mitochondria and ER contact phenotypes compared to the loss of *vps13d* alone (Figure 5I and J). These findings indicate that Vps13D and Vmp1 function in the same pathway to regulate mitophagy and mitochondria and ER contact, and that Vps13D functions downstream of Vmp1.

marf/MFN2 suppresses *vps13d* and *vmp1* mutant phenotypes

The role of Vps13D in regulating mitochondria and ER contact sites prompted us to consider the relationship between Vps13D and known regulators of inter-organelle contact. Mfn2 (Marf in flies) has been implicated in mitochondria and ER contact,[23-25] and knockdown of *marf* suppressed the *vps13d* knockdown mitochondria size phenotype.[7] Therefore, we investigated how loss of Vps13D influences Marf in *Drosophila*. Antibodies against Marf do not work for immunohistochemistry, but can be used for immunoblotting (Figure S6A). Therefore, we analyzed Marf levels in intestines isolated from control and *vps13d* mutant animals 2 hours after pupariation. Intestines from *vps13d (ΔUBA)/DF* trans-heterozygous mutants have increased levels of Marf and ATP5a compared to *vps13d (ΔUBA)*/+ and *Df/+* controls 2 hours after pupariation (Figure 6A and B), suggesting that Vps13D influences Marf levels. Similarly, patient fibroblasts incubated with mitochondrial uncoupler to induce mitophagy were unable to degrade ATP5a and MFN2 as effectively as heterozygous control fibroblasts even though MFN1 degradation was unaffected (Figure S6B and C).[8,9]

We next investigated if Marf interacts with Vps13D in *Drosophila.* The large size of Vps13D made it difficult to conduct biochemical experiments using exogenous expression in animal and cell culture models. Thus, we used CRISPR to tag the endogenous *Drosophila vps13d* gene with *3xflag* on the C terminus of the open reading frame (Figure S6D). Unlike *vps13d* mutants, these flies are viable, fertile, and do not have altered mitochondrial morphology in intestine cells at 2 hours after pupariation (Figure S6E). Co-staining of intestine cells with anti-FLAG and anti-Vps13D at 2 hours after pupariation revealed co-localization (Figure S6F). Furthermore, *vps13d-3xFLAG* pupal lysates had a unique band at the approximate weight of Vps13d-3xFLAG that was absent in the untagged *w1118* pupae (Figure S6G). The 3xFLAG epitope was used to immuno-precipitate Vps13D and potential interacting proteins. We used a Marf-specific antibody to reveal the presence of a band corresponding to

Author Manuscript Author Manuscript Author Manuscript Author Manuscript

endogenous Marf in the *vps13d-3xflag* eluate that was absent in the *w1118* negative control eluate (Figure S6H and I). We did not obtain significant enrichment of endogenous COXIV, an inner mitochondrial membrane protein serving as a control for non-specific mitochondrial protein interactions, in the *vps13d-3xFLAG* eluate. These results suggest a specific physical interaction between Vps13d and Marf.

We next sought to characterize the role that Marf may play in mitochondrial clearance in intestines 2 hour after pupariation. Interestingly, over-expression of Marf inhibited mitochondrial clearance (Figure 6C and D), a phenotype that is similar to *vps13d* loss-of-function mutants. Similar results were obtained by expression of Marf in all intestine enterocyte cells 2 hours after pupariation (Figure S6J). Unlike *vps13d* loss-of-function mutants, *marf(B)* loss-of-function mutant cells did not possess a defect in mitochondrial clearance (Figure 6E and F). In addition, *marf(B)* mutant cells did not have altered Vps13d puncta (Figure 6G and H), suggesting that Vps13D functions upstream of Marf in the regulation mitochondrial clearance and morphology.

MFN2 is an established mitochondria and ER tether that regulates mitochondrial dynamics and mitophagy.[23-25] Given the physical and genetic relationship between Vps13d, Vmp1, and Marf, we hypothesized that Vmp1 and Vps13D may regulate mitochondria morphology and mitochondria and ER contact sites upstream of Marf. Knockdown of *marf* suppressed the enlarged mitochondrial phenotypes seen in *vps13d (ΔUBA/MiMic)* mutants and *vmp1* knockdown intestine cells (Figure 7A and B). Knockdown of *marf* also suppressed the Mito-QC and Ref2p accumulation phenotype in *vps13d* mutant intestine cells (Figure S7A and B). Consistent with findings in other cell lines,[22] knockdown of *VMP1* in heterozygous control fibroblasts increased the number of round mitochondria, similar to the *VPS13D* mutant patient-derived fibroblasts. *VMP1* knockdown in patient-derived fibroblasts did not significantly increase the ratio of round mitochondria to tubular mitochondria, suggesting that like in *Drosophila* intestines, *VMP1* and *VPS13D* are functionally linked in a pathway in human fibroblasts. Significantly, *MFN2* knockdown in patient-derived fibroblasts (Figure S7C) also suppressed the abnormal mitochondrial phenotype in *VPS13D* mutant patient-derived fibroblasts (Figure 7C and D). Interestingly, *MFN1* knockdown in patient-derived fibroblasts (Figure S7C) did not suppress this *VPS13D* associated phenotype (Figure 7C and D). These findings suggest that the mechanistic relationship between *VPS13D, VMP1*, and *Marf/MFN2* are conserved from *Drosophila* to humans, and that this relationship likely contributes to disease pathology.

We next investigated if decreased *marf/MFN2* function can suppress the *vps13d* mutant intestine cell mitochondria and ER contact phenotype. Consistent with our previous TEM analyses of mitochondria in *vps13d* RNAi-expressing intestine cells,[7] reduction of *marf* function by RNAi suppresses the enlarged mitochondrial phenotype in *vps13d (ΔUBA)/MiMic* mutants (Figure 7E and F). Significantly, expression of *marf* RNAi also suppressed the increased mitochondria and ER contact phenotype in *vps13d* mutant intestine cells (Figure 7E and G). Importantly, *MFN2* knockdown in *VPS13D* mutant fibroblasts also suppressed the mitochondria and ER contact phenotype (Figure 7E and H). Therefore, these data indicate that Vps13d mechanistically regulates mitochondria and ER contact sites through Marf/MFN2 in *Drosophila* and human fibroblasts.

Author Manuscript Author Manuscript Author Manuscript Author Manuscript

DISCUSSION

Mitophagy plays an important role in organism health and disease. *vps13d* is not only a regulator of mitophagy, but is also required for proper mitochondrial morphology.[7] However, the pathway and mechanism by which *vps13d* regulates mitochondrial size and clearance, and subsequently why *vps13d* is crucial for cell health and its associated diseases, remains elusive. Here, we establish *vmp1* as a regulator of *vps13d* mediated mitophagy and regulation of mitochondria morphology. In doing so, we identify a new function of Vps13D as a regulator of mitochondria and ER contact in multiple systems, including fibroblasts derived from patients with vps13d-associated neurological symptoms.

The regulation of mitochondria and ER contact sites plays important roles in autophagy and mitochondrial morphology. Autophagosomes form at mitochondria and ER contact sites,[26] making these sites crucial for autophagy. In yeast, it has been shown that mitochondria and ER contact sites are required for mitophagy.[27] Furthermore, mitochondria and ER contact regulate mitochondrial dynamics in cultured human cells,[28] and altered mitochondrial dynamics influences *vps13d* mutant intestine cell mitochondrial size and clearance.[7] The inability to disassemble mitochondria and ER contact sites, such as is required in Pink1/Parkin mitophagy,[25] can explain the mitophagy deficiency and altered mitochondrial morphology phenotypes that we observe in diverse *vps13d* mutant models.

Here we have identified the first direct link between Vmp1 and the Vps13D family. Vmp1 is an ER localized transmembrane protein that regulates autophagy through disassembly of inter-organelle membrane contacts, where loss of Vmp1 leads to failure in the disassembly of these contact sites.[22] Vps13d interacts with proteins that localize to mitochondria and ER contact sites, including Marf.[23,29,30] Consistent with our data in *Drosophila*, Vps13D was recently reported to interact with Mfn2 in 293 human embryonic kidney cells.[29] Marf has been linked to mitophagy by being degraded by the PINK1/PARKIN pathway.[25, 31,] It may thus be possible that Vps13dfacilitates Marf degradation to decrease mitochondria and ER contact sites, enabling better access for Pink1/Parkin substrates during mitophagy.[25] Recent studies have shown that other proteins known to regulate mitophagy and mitochondrial dynamics also localize to mitochondria and ER contact sites.[29,30] Along with Marf, these proteins provide a possible mechanism by which Vps13d regulates mitophagy and mitochondrial morphology.

Our data indicate that Vps13d functions as a link between Vmp1 and regulators of mitochondrial dynamics, such as Marf. In mammalian cell lines, failure to disassemble mitochondria and ER contact sites is believed to contribute to the abnormal spherical mitochondria in *vmp1* mutant cells.[22] Similarly, *VPS13D* mutant HeLa cells display a spherical mitochondrial morphology.[7] Vmp1 is an integral ER membrane protein and localization is unlikely to be affected by Vps13D function,[21] and this is consistent with our findings (Figure 5C and D). Since Vps13d acts downstream of Vmp1, it is thus likely that Vps13d helps mediate disassembly of membranes at mitochondria and ER contact sites via a mechanism that is similar to Vmp1. Thus, Vps13d may function at a nodal point that links mitochondria and ER contact to influence both mitochondrial dynamics and mitophagy, processes that are mostly studied in isolation. Curiously, Vmp1 also regulates membrane

Author Manuscript Author Manuscript Author Manuscript Author Manuscript

contacts between the ER and other organelles, including endosomes and lipid droplets. The influence of Vmp1 on these organelles does not appear to impact autophagy, suggesting that Vmp1 also has autophagy-independent functions.[22] Furthermore, unlike Vps13D, Vmp1 appears to be required for starvation induced autophagy.[7,22] Thus, while Vps13D appears to function downstream of Vmp1 in some cellular contexts, it is likely that Vmp1-dependent and Vps13D-independent processes exist. Investigation of the mechanism by which Vmp1 affects Vps13D puncta localization, including if Vmp1 regulates Vps13D protein levels or stability, may clarify this relationship between Vps13D and Vmp1. Furthermore, while we have focused on the role of Vps13D and Vmp1 in mitophagy, there remains the possibility that these proteins are also responsible for the clearance of other cargos.

Vps13 family members are known to act as lipid transfer proteins.[14,32] Autophagosomes form at mitochondria and ER contact sites, and lipids from both organelles are thought to contribute to the autophagosome membrane.[26,33] As a lipid transporter, Vps13D could facilitate the transfer of important lipids to the forming autophagosome membrane. Given the importance of lipid transfer in organelle signaling pathways,[34] Vps13D could also play a role in membrane disassembly by allowing the formation of the autophagosome between the mitochondria and ER.

vps13d loss-of-function mutant phenotypes are different than those of other *VPS13* family members. Knockdown of *VPS13A* in cell lines results in decreased mitochondria and ER contact, these cells do not have spherical mitochondria, which is in direct contrast to phenotypes in *VMP1* and *VPS13D* mutant cells.[22,35] Furthermore, VPS13C does not localize to mitochondria and ER contact sites.[14] These findings suggest VMP1 functions in a pathway with VPS13D, but not other VPS13 family members. In *Drosophila*, only loss of *vps13d*, and neither *vps13a* nor *vps13b*, results in the same autophagy deficiency phenotype as loss of *vmp1*.[7] In addition to being the only VPS13 family member that is essential for survival, VPS13D is the only VPS13 protein with a ubiquitin binding domain, which is crucial for regulating mitochondria morphology and clearance. Even the single yeast VPS13 does not have this ubiquitin binding domain,[7,13] hinting that the divergence of VPS13D from other VPS13 family members may have been the result of an evolutionary need for regulating more complex functions in higher life forms. These observations further illustrate the unique role that VPS13D plays compared to other VPS13 family members.

Mitochondria and ER contact sites are responsible for a wide range of cellular processes. In addition to autophagy, these sites are crucial for mitochondrial biogenesis, stress response, lipid exchange, calcium signaling, intracellular trafficking and immune responses.[36] As many cells depend on these processes, it is possible that mitochondria and ER contact disruption in *vps13d* mutants is why *vps13d* is such an essential gene (Figure S1A).[7] Furthermore, Vps13D could regulate membrane contact sites between other organelles, potentially increasing the number of vital roles of Vps13D. For example, over-expression of a peroxisome-localizing variant of Miro increased recruitment of Vps13D to peroxisomes in COS7 cells.[37] These findings suggest that in addition to mitophagy, there are still uncharacterized and context-dependent functions of Vps13D.

Author Manuscript Author Manuscript Author Manuscript Author Manuscript

Dysfunction of mitochondria and ER contacts is believed to contribute to neurodegenerative conditions through impairment of these processes.[28,38-40] Individuals with *VPS13D* mutations possess a range of symptoms, from asymptomatic to early childhood onset neurological disabilities,[10, 11] raising the possibility that the severity of disease may be proportional to the extent of altered mitochondria and ER contact. Knockdown of *vps13d* in *Drosophila* neurons results in enlarged mitochondria, consistent with Vps13D playing a role in neurological health in *Drosophila*.[41] There are no known treatments for patients experiencing symptoms from *VPS13D* mutation-driven diseases. However, the relationship between *vps13d* and *marf/mfn2* raises the possibility that therapies designed to reduce MARF/MFN2 activity could alleviate such symptoms. The link between *vps13d* and *vmp1* also raises the novel possibility that *VMP1* may play a role in neurological disease. This link not only includes the diseases *VPS13D* is involved in, but unique diseases that *MFN2* is involved in, such as Charcot-Marie-Tooth disease.[42] Future studies will determine if the membrane contact function of *vps13d* and relationship to either *vmp1* or *marf/MFN2* contributes to other associated diseases.

STAR METHODS

RESOURCE AVAILABILITY

Lead Contact—Please contact the Lead Contact, Dr. Eric Baehrecke, for additional information and requests for resources and reagents (eric.baehrecke@umassmed.edu).

Materials Availability—Please contact the Lead Contact to request all strains and protocols pertaining to this study.

Data and Code Availability—Please contact the Lead Contact to obtain any data or related images generated in this study.

EXPERIMENTAL MODELS AND SUBJECT DETAILS

Drosophila* strains—Drosophila melanogaster* strains used in this study are listed in the Key Resources Table. *Drosophila* strains used for each experiment are listed in Table S1. w^{1118} were used as controls. All flies were raised on standard cornmeal/molasses/agar media at 25°C.

Human cell lines—All cells used in this study are listed in Key Resources Table. Cells were cultured at 37°C in 5% CO_2 in DMEM supplemented with 5% FBS and Penicillin/Streptomycin, as previously described.[7] *VPS13D* mutant HeLa cells were designed as previously described.[7] Fibroblasts from patients with *VPS13D* mutations were obtained and cultured as described.[10] Cells were transfected with the Lipofectamine™ RNAiMAX Transfection Reagent (Invitrogen) following manufacturer protocol and processed 2 days later.

METHOD DETAILS

vmp1(Δ), gfp-vmp1, and vps13d-3xFLAG* fly construction—vmp1* loss-of-function, *vmp1(Δ)* and N terminal GFP-tagged (*gfp-vmp1) vmp1* strains were edited using CRISPR/

Author Manuscript Author Manuscript Author Manuscript Author Manuscript

Cas9.[43] All germline injections were done by the UMass Medical School CRISPR Core. Oligonucleotide donor used to design *gfp-vmp1* is listed in Table S2. All other primers and oligonucleotides used in this study are listed in the Key Resources Table. For *vmp1(Δ)*, the following sgRNA targeting sequences were used (5' to 3'): sgRNA1: TGTTGTTGTGACGATTGCTC, sgRNA2: TTACGGGACTAGAAAATCAG. A 200bp ultramer donor with 100bp regions flanking the site of the deletion designed by IDT (San Diego, California) was used to facilitate the deletion, resulting in a single female fly with the deletion that was validated by DNA sequence. Dp(1;3)RC025 from the Bloomington Duplication Project was used to verify that lethality was due to loss of the *vmp1*. For *gfp-vmp1*, the following sgRNA targeting sequences were used (5' to 3'): sgRNA3: TGCTGTGACATTTAAGCGGT, sgRNA4: CGAATGCTGTGACATTTAAG. A 2kb gblock with 1kb regions flanking the site of insertion and the GFP open reading frame was designed by IDT (San Diego, California) and used to tag the N terminal of *vmp1* with *gfp*. A single female fly containing the insertion was collected, and validated by DNA sequencing. For vps13d-3xflag, the following sgRNA targeting sequence was used (5' to 3'): sgRNA5:TTTATAAAATGCAATAGGT. A 2kb region flanking the C terminal of genomic *vps13d* was amplified by PCR and site-directed mutagenesis was used to insert the 3xflag sequence in frame immediately before the stop codon. This fragment was inserted into a TOPO vector via TOPO cloning and sequenced to ensure no additional mutations were present and was used to tag the C terminal of vps13d with 3xflag. A single female fly containing the insertion was collected and validated by DNA sequencing.

Induction of mosaic RNAi/mutant cell clones and whole intestine RNAi expression—Mosaic GFP positive RNAi- and transgene-expressing cell clones and fluorescentnegative cell clones were induced as described.[7] To induce mosaic *vmp1(Δ)* and *vps13d(MiMic)* loss-of-function mutant cell clones, we used the *hsflp, FRT19A, mRFP* and *hsflp;;FRT2A, Ubi-nlsGFP* flies and crossed them with *vmp1(Δ) FRT19A/ FM7i-pAct-GFP* and *vps13d(MiMic) FRT2A/TM6B* flies, respectively. Mosaic clonal analyses were only used as indicated, otherwise entire mutant or organ specific RNAi animals were used. 8-hour eggs lays were heat shocked for 90 minutes at 37°C. Myo31DFNP0001 (NP1-GAL4) was used to drive expression of transgenes, including RNAi and the MitoQC reporter, throughout the entire larval intestine.[44]

Dissection and immuno-labeling of Drosophila larval intestines and Cell Lines —White prepupae were collected and allowed to develop on wet filter paper for 2 hours prior to dissection. Intestines were immuno-stained as previously described with modifications.[7] Intestines were removed in cold PBS before being placed in 4% paraformaldehyde solution for fixation at 4°C overnight. Intestines were washed twice with PBS and then twice with 0.1% PBSTx before blocking in 5% normal goat serum for 90 minutes and incubation with primary antibody in 0.1% PBSTx overnight. Intestines were then stained with secondary antibody for 3 hours before nuclei staining and mounting. All antibodies used in this study are listed in Key Resources Table. The following primary antibodies were used: rabbit anti-ref(2)p (1:1000, from Gabor Juhasz), mouse anti-ATP synthase complex V (1:1000, Abcam #ab14748), anti-GFP (1:1000, Abcam # ab13970), rabbit anti-TOMM20 (1:200, Abcam # ab78547), rabbit anti-SERCA (1:1000, from Mani

Author Manuscript Author Manuscript Author Manuscript Author Manuscript

Ramaswami), rabbit anti-FLAG (1:1000, Abcam #Ab1162), and anti-Vps13D (1:50).[7] The following secondary antibodies were used: anti-mouse AlexaFluor 647 (Invitrogen #A-21235), anti-rabbit Alexafluor 546 (Invitrogen # A-11035) and anti-chicken AlexaFluor 488 (#A-11039). Nuclei were stained with Hoescht (Invitrogen) and samples were mounted with Vectashield (Vector Lab). Intestines expressing mCherryAtg8a puncta driven by the Atg8a promoter were fixed overnight at 4°C in 4% paraformaldehyde before being imaged the next day.[45] Cell lines were fixed in 4% paraformaldehyde for 30 minutes at room temperature, permeabilized with digitonin for 15 minutes, and blocked in 5% normal goat serum in PBS before overnight staining with primary antibody overnight at 4°C. Cells were then washed and stained with secondary antibody before mounting in Vectashield with DAPI. Images were acquired using a Zeiss LSM 700 Axioobserver confocal microscope with Plan apochromate 63x/1.40 NA oil immersion objective. Signal in images were thresholded to only include distinct puncta and gaussian blur with sigma 0.8 was applied to reduce background noise. Puncta were quantified using Fiji (ImageJ) and only the brightest 2.5% of puncta were included in quantification.

Transmission electron microscopy—Transmission electron microscopy (TEM) was conducted as previously described with modifications.[7] Intestines were dissected in PBS (GIBCO) 2 hours after pupariation and fixed in a solution of 2.5% glutaraldehyde and 2% paraformaldehyde in 0.1M sodium cacodylate buffer, pH 7.4 (Electron Microscopy Sciences) for 1 hour at room temperature followed by overnight fixation at 4°C in fresh fix. Intestines were washed in 0.1M sodium cacodylate buffer, pH 7.4, post-fixed in 1% osmium tetroxide in distilled water for 1 hour at room temperature and washed in distilled water. Preparations were stained en bloc in 1% aqueous uranyl acetate for 1 hour at 4°C in the dark, washed in distilled water, dehydrated through a graded ethanol series, treated with propylene oxide and infiltrated in SPI-pon/Araldite for embedding. We cut ultrathin sections on a Leica UC7 microtome. Sections were stained with uranyl acetate and lead citrate and examined on a Phillips CM10 TEM. Images were taken down the length of the anterior region of the midgut to ensure an unbiased approach. For each genotype, at least 3 intestines were embedded and sectioned for analyses and quantification. We reviewed all images and selected representative images for analyses.

For cell culture, plated cells were prefixed in 50% media: 50% fix, 2.5% glutaraldehyde and 2% paraformaldehyde in 0.1M sodium cacodylate buffer, pH 7.4 (Electron Microscopy Sciences) for 5 minutes followed by fixation in full fix for 1 hour at room temperature. Cells were then washed with 0.1M cacodylate buffer, pH 7.4, post-fixed in 1% osmium tetroxide in distilled water for 1 hour at room temperature and washed in distilled water. Preparations were stained en bloc in 1% aqueous uranyl acetate over night at 4°C in the dark and then washed in distilled water. The cells were then scraped and pelleted. Cell pellets were embedded in agarose, dehydrated through a graded ethanol series, treated with propylene oxide and infiltrated in SPI-pon/Araldite for embedding. We cut ultrathin sections on a Leica UC7 microtome. Sections were stained with uranyl acetate and lead citrate and examined on a Phillips CM10 TEM. For each cell line, at least (3) 10 cm^2 dishes at 60-80% confluency were embedded independently of each other and sectioned in an unbiased manner for analyses and quantification.

Author Manuscript Author Manuscript Author Manuscript Author Manuscript

Western Blot and Immunoprecipitation—Tissue was lysed in 1X Laemli Sample Buffer diluted in RIPA lysis buffer (10mM Tris-Cl PH 8.0, 1mM EDTA PH 8.0, 0.5mM EGTA, 2.4mM Sodium Deoxycholate 140mM Sodium Chloride) at a ratio of 10μL lysis buffer per intestine and 30μL per whole pupa. Samples were crushed in solution using a plastic pestle for 30 seconds before being boiled at 99°C for 6 minutes. Samples were run on 7.5% polyacrylamide gel, transferred onto 0.45μm PVDF membranes (Millipore Sigma), and probed with antibodies using standard protocols. Primary antibodies used were mouse anti-FLAG (1:1000, Millipore Sigma), rabbit anti-Marf (1:1000, from Alexander Whitworth) mouse anti-CoxIV (1:1000, Abcam), mouse anti-Actin (1:1000, Proteintech), mouse anti-MFN2 (1:1000, Abnova #H00009927-M03), anti-MFN1 (1:1000, Proteintech #13798-1-AP) mouse anti-ATP synthase complex V (1:1000, Abcam).

For immunoprecipitations, 2-hour-old pupae were lysed in RIPA lysis buffer supplemented with 1mM NEM, 1mM PMSF and Halt Protease Inhibitor Cocktail (Thermo Fisher) at a ratio of 16 pupae per 250μL lysis buffer. Pupae were crushed with a plastic pestle for 30 seconds and incubated on ice for 30 minutes before being centrifuged at 4°C at 13,000rpm for 10 minutes. Supernatant was filtered through 0.45μm Cellulose Acetate filters (Millipore Sigma). 30μL of filtered supernatant was diluted in 10μL of 4x Laemli Sample Buffer (Biorad), boiled for 6 minutes at 99°C and used as input. 200μL of filtered supernatant (approximately 1mg protein) was used for immunoprecipitation. 40μL of anti-FLAG M2 magnetic bead slurry (Millipore Sigma) warmed to room temperature was washed twice with RIPA buffer before incubation with filtered supernatant for 2 hours at 4°C on a rotator. Following incubation, supernatant was discarded and beads were washed 4 times with 1mL 0.1% PBST. Beads were eluted with 20μL 1X Laemli Sample Buffer diluted in RIPA lysis buffer and boiled for 6 minutes at 99°C. 20μL of input and eluate was run on 7.5% polyacrylamide gel for Western Blot analysis.

QUANTIFICATION AND STATISTICAL ANALYSES

Quantification of mitochondria morphology in fibroblasts were blindly characterized as tubular or spherical. All other quantifications, including cell size and puncta in immunofluorescence images were conducted using ImageJ, as described previously.[7] Sample sizes (n) in immunofluorescent experiment quantifications represent number of cells.

TEM analyses of mitochondria area was manually calculated by individually analyzing mitochondria using ImageJ. For determination of mitochondria and ER contact sites, mitochondria and ER were individually identified on TEM sections and distance between mitochondria and ER was manually measured using ImageJ. Regions of ER that were within 30nm of mitochondria and had a contact length of at least 20nm were identified as mitochondria and ER contact sites as previously defined.[22] The length of these sites of contact were manually measured for each mitochondria and compared with the entire mitochondria perimeter to determine the percentage in contact. Regions for analyses were randomly selected from embedded blocks for each sample. For each analysis, at least 50 mitochondria from at least 20 sections and 3 independent experiments were used for quantifications. Sample sizes (n) for TEM quantifications represent number of mitochondria.

Author Manuscript Author Manuscript Author Manuscript Author Manuscript

All experiments are representative of 3 independent replicates. No statistical methods were used to predetermine sample sizes. Preliminary experiments were conducted to achieve similar sample sizes as previous published studies using our model systems. Animals were not excluded for statistical analyses. Researchers were not blinded. Unless otherwise stated, p values were calculated using the two-tailed student t-test without Welch's correlation for experiments where a single comparison was made. For experiments with multiple comparisons, p values were calculated using one-way ANOVA with Tukey post-hoc analysis. p values greater than 0.05 were considered non-significant (n.s.). All bars are means and error bars are SEM unless otherwise.

Supplementary Material

Refer to Web version on PubMed Central for supplementary material.

Acknowledgments

We thank the Baehrecke laboratory, R. Youle, C. Wang, G. Juhasz, M. Ramaswami, A.J. Whitworth, A. Woloszynska, the Vienna Drosophila Resource Center, the Bloomington Stock Center, the Kyoto Drosophila Genetic Resource Center, and the Electron Microscopy Core Facility at UMass Medical School for advice, flies, antibodies, cell lines and technical support. We would like to thank the VPS13D-patients and their relatives, and K. Lohmann, J.E. Gudjonsson,, E. Seong, and L. Gates with establishing or maintaining iPSCs of VPS13D patients and relatives. This work was supported by R35GM131689 to E.H.B. and F30CA239374 to J.L.S.

REFERENCES

1. Palikaras K, Lionaki E, and Tavernarakis N (2018). Mechanisms of mitophagy in cellular homeostasis, physiology and pathology. Nat Cell Biol 20, 1013–1022. [PubMed: 30154567]
2. Wang Y, Liu N, and Lu B (2019). Mechanisms and roles of mitophagy in neurodegenerative diseases. CNS Neurosci Ther 25, 859–875. [PubMed: 31050206]
3. Narendra DP, Jin SM, Tanaka A, Suen D-F, Gautier CA, Shen J, Cookson MR, and Youle RJ (2010). PINK1 Is Selectively Stabilized on Impaired Mitochondria to Activate Parkin. PLoS Biol 8, e1000298. [PubMed: 20126261]
4. McWilliams TG, Prescott AR, Montava-Garriga L, Ball G, Singh F, Barini E, Muqit MMK, Brooks SP, and Ganley IG (2018). Basal Mitophagy Occurs Independently of PINK1 in Mouse Tissues of High Metabolic Demand. Cell Metab 27, 439–449. [PubMed: 29337137]
5. Lee JJ, Sanchez-Martinez A, Zarate AM, Benincá C, Mayor U, Clague MJ, and Whitworth AJ (2018). Basal mitophagy is widespread in Drosophila but minimally affected by loss of Pink1 or parkin. J Cell Biol 217, 1613–1622. [PubMed: 29500189]
6. Chang T-K, Shravage BV, Hayes SD, Powers CM, Simin RT, Harper JW, and Baehrecke EH (2013). Uba1 functions in Atg7- and Atg3-independent autophagy. Nat Cell Biol 15, 1067–1078. [PubMed: 23873149]
7. Anding AL, Wang C, Chang T-K, Sliter DA, Powers CM, Hofmann K, Youle RJ, and Baehrecke EH (2018). Vps13D Encodes a Ubiquitin-Binding Protein that Is Required for the Regulation of Mitochondrial Size and Clearance. Curr Biol 28, 287–295. [PubMed: 29307555]
8. Lee CY, Cooksey BA, and Baehrecke EH (2002). Steroid regulation of midgut cell death during Drosophila development. Dev Biol 250, 101–111. [PubMed: 12297099]
9. Jiang C, Baehrecke EH, and Thummel CS (1997). Steroid regulated programmed cell death during Drosophila metamorphosis. Development 124, 4673–4683. [PubMed: 9409683]
10. Seong E, Insolera R, Dulovic M, Kamsteeg E-J, Trinh J, Brüggemann N, Sandford E, Li S, Ozel AB, Li JZ, et al. (2018). Mutations in VPS13D lead to a new recessive ataxia with spasticity and mitochondrial defects. Ann Neurol 83, 1075–1088. [PubMed: 29604224]

Author Manuscript Author Manuscript Author Manuscript Author Manuscript

11. Gauthier J, Meijer IA, Lessel D, Mencacci NE, Krainc D, Hempel M, Tsiakas K, Prokisch H, Rossignol E, Helm MH, et al. (2018). Recessive mutations in VPS13D cause childhood onset movement disorders. Ann Neurol 83, 1089–1095. [PubMed: 29518281]
12. Brickner JH, and Fuller RS (1997). SOI1 encodes a novel, conserved protein that promotes TGN-endosomal cycling of Kex2p and other membrane proteins by modulating the function of two TGN localization signals. J Cell Biol 139, 23–36. [PubMed: 9314526]
13. Velayos-Baeza A, Vettori A, Copley RR, Dobson-Stone C, and Monaco AP (2004). Analysis of the human VPS13 gene family. Genomics 84, 536–549. [PubMed: 15498460]
14. Kumar N, Leonzino M, Hancock-Cerutti W, Horenkamp FA, Li P, Lees JA, Wheeler H, Reinisch KM, and De Camilli P (2018). VPS13A and VPS13C are lipid transport proteins differentially localized at ER contact sites. The Journal of cell biology 217, 3625–3639. [PubMed: 30093493]
15. John Peter AT, Herrmann B, Antunes D, Rapaport D, Dimmer KS, and Kornmann B (2017). Vps13-Mcp1 interact at vacuole-mitochondria interfaces and bypass ER-mitochondria contact sites. J Cell Biol 216, 3219–3229. [PubMed: 28864540]
16. Blomen VA, Májek P, Jae LT, Bigenzahn JW, Nieuwenhuis J, Staring J, Sacco R, van Diemen FR, Olk N, Stukalov A, et al. (2015). Gene essentiality and synthetic lethality in haploid human cells. Science 350, 1092. [PubMed: 26472760]
17. Wang T, Birsoy K, Hughes NW, Krupczak KM, Post Y, Wei JJ, Lander ES, and Sabatini DM (2015). Identification and characterization of essential genes in the human genome. Science 350, 1096–1101. [PubMed: 26472758]
18. Nakada TA, Boyd JH, Russell JA, Aguirre-Hernandez R, Wilkinson MD, Thair SA, Nakada E, McConechy MK, Fjell CD, and Walley KR (2015). VPS13D Gene Variant Is Associated with Altered IL-6 Production and Mortality in Septic Shock. J Innate Immun 7, 545–553. [PubMed: 25896417]
19. Bousquet M, Noirot C, Accadbled F, Sales de Gauzy J, Castex MP, Brousset P, and Gomez-Brouchet A (2016). Whole-exome sequencing in osteosarcoma reveals important heterogeneity of genetic alterations. Ann Oncol 27, 738–744. [PubMed: 26787232]
20. Andersen JN, Sathyanarayanan S, Di Bacco A, Chi A, Zhang T, Chen AH, Dolinski B, Kraus M, Roberts B, Arthur W, et al. (2010). Pathway-Based Identification of Biomarkers for Targeted Therapeutics: Personalized Oncology with PI3K Pathway Inhibitors. Sci Transl Med 2, 43ra55.
21. Tian Y, Li Z, Hu W, Ren H, Tian E, Zhao Y, Lu Q, Huang X, Yang P, Li X, et al. (2010). C. elegans Screen Identifies Autophagy Genes Specific to Multicellular Organisms. Cell 141, 1042–1055. [PubMed: 20550938]
22. Zhao YG, Chen Y, Miao G, Zhao H, Qu W, Li D, Wang Z, Liu N, Li L, Chen S, et al. (2017). The ER-Localized Transmembrane Protein EPG-3/VMP1 Regulates SERCA Activity to Control ER-Isolation Membrane Contacts for Autophagosome Formation. Mol Cell 67, 974–989. [PubMed: 28890335]
23. de Brito OM, and Scorrano L (2008). Mitofusin 2 tethers endoplasmic reticulum to mitochondria. Nature 456, 605–610. [PubMed: 19052620]
24. Naon D, Zaninello M, Giacomello M, Varanita T, Grespi F, Lakshminaranayan S, Serafini A, Semenzato M, Herkenne S, Hernández-Alvarez MI, et al. (2016).Critical reappraisal confirms that Mitofusin 2 is an endoplasmic reticulum-mitochondria tether. Proc Natl Acad Sci U S A 113, 11249–11254. [PubMed: 27647893]
25. McLelland G-L, Goiran T, Yi W, Dorval G, Chen CX, Lauinger ND, Krahn AI, Valimehr S, Rakovic A, Rouiller I, et al. (2018). Mfn2 ubiquitination by PINK1/parkin gates the p97-dependent release of ER from mitochondria to drive mitophagy. Elife 7, e32866. [PubMed: 29676259]
26. Hamasaki M, Furuta N, Matsuda A, Nezu A, Yamamoto A, Fujita N, Oomori H, Noda T, Haraguchi T, Hiraoka Y, et al. (2013). Autophagosomes form at ER–mitochondria contact sites. Nature 495, 389. [PubMed: 23455425]
27. Böckler S, and Westermann B (2014). Mitochondrial ER Contacts Are Crucial for Mitophagy in Yeast. Dev Cell 28, 450–458. [PubMed: 24530295]
28. Friedman JR, Lackner LL, West M, DiBenedetto JR, Nunnari J, and Voeltz GK (2011). ER tubules mark sites of mitochondrial division. Science 334, 358–362. [PubMed: 21885730]

Author Manuscript Author Manuscript Author Manuscript Author Manuscript

29. Antonicka H, Lin Z-Y, Janer A, Aaltonen MJ, Weraarpachai W, Gingras A-C, and Shoubridge EA (2020). A High-Density Human Mitochondrial Proximity Interaction Network. Cell Metab 32, 479–497. [PubMed: 32877691]

30. Hung V, Lam SS, Udeshi ND, Svinkina T, Guzman G, Mootha VK, Carr SA, and Ting AY (2017). Proteomic mapping of cytosol-facing outer mitochondrial and ER membranes in living human cells by proximity biotinylation. Elife 6, e24463. [PubMed: 28441135]

31. Ziviani E, Tao RN, and Whitworth AJ (2010). Drosophila parkin requires PINK1 for mitochondrial translocation and ubiquitinates mitofusin. Proc Natl Acad Sci U S A 107, 5018–5023. [PubMed: 20194754]

32. Gao M, and Yang H (2018). VPS13: A lipid transfer protein making contacts at multiple cellular locations. J Cell Biol 217, 3322–3324. [PubMed: 30181317]

33. Hailey DW, Rambold AS, Satpute-Krishnan P, Mitra K, Sougrat R, Kim PK, and Lippincott-Schwartz J (2010). Mitochondria supply membranes for autophagosome biogenesis during starvation. Cell 141, 656–667. [PubMed: 20478256]

34. Muallem S, Chung WY, Jha A, and Ahuja M (2017). Lipids at membrane contact sites: cell signaling and ion transport. EMBO Rep 18, 1893–1904. [PubMed: 29030479]

35. Yeshaw WM, van der Zwaag M, Pinto F, Lahaye LL, Faber AIE, Gómez-Sánchez R, Dolga AM, Poland C, Monaco AP, van Ijzendoorn SCD, et al. (2019). Human VPS13A is associated with multiple organelles and influences mitochondrial morphology and lipid droplet motility. Elife 8, e43561. [PubMed: 30741634]

36. Paillusson S, Stoica R, Gomez-Suaga P, Lau DHW, Mueller S, Miller T, and Miller CCJ (2016). There's Something Wrong with my MAM; the ER-Mitochondria Axis and Neurodegenerative Diseases. Trends Neurosci 39, 146–157. [PubMed: 26899735]

37. Guillén-Samander A, Leonzino M, Hanna MG, Tang N, Shen H, and De Camilli P (2021). VPS13D bridges the ER to Miro containing membranes. bioRxiv, 2020.2010.2007.328906.

38. Chakrabarti R, Ji W-K, Stan RV, de Juan Sanz J, Ryan TA, and Higgs HN (2018). INF2-mediated actin polymerization at the ER stimulates mitochondrial calcium uptake, inner membrane constriction, and division. J Cell Biol 217, 251–268. [PubMed: 29142021]

39. Giorgi C, Missiroli S, Patergnani S, Duszynski J, Wieckowski MR, and Pinton P (2015). Mitochondria-associated membranes: composition, molecular mechanisms, and physiopathological implications. Antioxid Redox Signal 22, 995–1019. [PubMed: 25557408]

40. Schon EA, and Area-Gomez E (2013). Mitochondria-associated ER membranes in Alzheimer disease. Mol Cell Neurosci 55, 26–36. [PubMed: 22922446]

41. Insolera R, Lőrincz P, Wishnie AJ, Juhasz G, and Collins CA (2020). Mitochondrial fission, integrity and completion of mitophagy require separable functions of Vps13D in *Drosophila* neurons. bioRxiv, 2020.2001.2021.914523.

42. Houlden H, and Reilly MM (2006). Molecular genetics of autosomal-dominant demyelinating Charcot-Marie-Tooth disease. Neuromolecular Med 8, 43–62. [PubMed: 16775366]

43. Gratz SJ, Ukken FP, Rubinstein CD, Thiede G, Donohue LK, Cummings AM, and O'Connor-Giles KM (2014). Highly specific and efficient CRISPR/Cas9-catalyzed homology-directed repair in Drosophila. Genetics 196, 961–971. [PubMed: 24478335]

44. Hayashi S, Ito K, Sado Y, Taniguchi M, Akimoto A, Takeuchi H, Aigaki T, Matsuzaki F, Nakagoshi H, Tanimura T et al. (2002). GETDB, a database compiling expression patterns and molecular locations of a collection of gal4 enhancer traps. Genesis 34, 58–61. [PubMed: 12324948]

45. Denton D, Chang TK, Nicolson S, Shravage B, Simin R, Baehrecke EH, and Kumar S (2012). Relationship between growth arrest and autophagy in midgut programmed cell death in Drosophila. Cell Death Differ 19, 1299–1307. [PubMed: 22555456]

46. Pircs K, Nagy P, Varga A, Venkei Z, Erdi B, Hegedus K, and Juhasz G (2012). Advantages and limitations of different p62-based assays for estimating autophagic activity in Drosophila. PLoS One 7, e44214–e44214. [PubMed: 22952930]

47. Sanyal S, Consoulas C, Kuromi H, Basole A, Mukai L, Kidokoro Y, Krishnan KS, and Ramaswami M (2005). Analysis of conditional paralytic mutants in Drosophila sarco-endoplasmic reticulum

Author Manuscript Author Manuscript Author Manuscript Author Manuscript

calcium ATPase reveals novel mechanisms for regulating membrane excitability. Genetics 169, 737–750. [PubMed: 15520268]

48. Dempster JM, Rossen J, Kazachkova M, Pan J, Kugener G, Root DE, and Tsherniak A (2019). Extracting Biological Insights from the Project Achilles Genome-Scale CRISPR Screens in Cancer Cell Lines. bioRxiv, 720243.

49. Meyers RM, Bryan JG, McFarland JM, Weir BA, Sizemore AE, Xu H, Dharia NV, Montgomery PG, Cowley GS, Pantel S, et al. (2017). Computational correction of copy number effect improves specificity of CRISPR-Cas9 essentiality screens in cancer cells. Nat Genet 49, 1779–1784. [PubMed: 29083409]

Author Manuscript Author Manuscript Author Manuscript Author Manuscript

Highlights

- Vps13D and Vmp1 are linked as regulators of autophagy and mitochondrial morphology
- Vps13D, like Vmp1, regulates mitochondria and ER contact sites
- Vps13D regulates mitophagy and mitochondrial morphology downstream of Vmp1
- Vps13D mitochondria and ER contact phenotypes depend on Marf/MFN2

Author Manuscript Author Manuscript Author Manuscript Author Manuscript

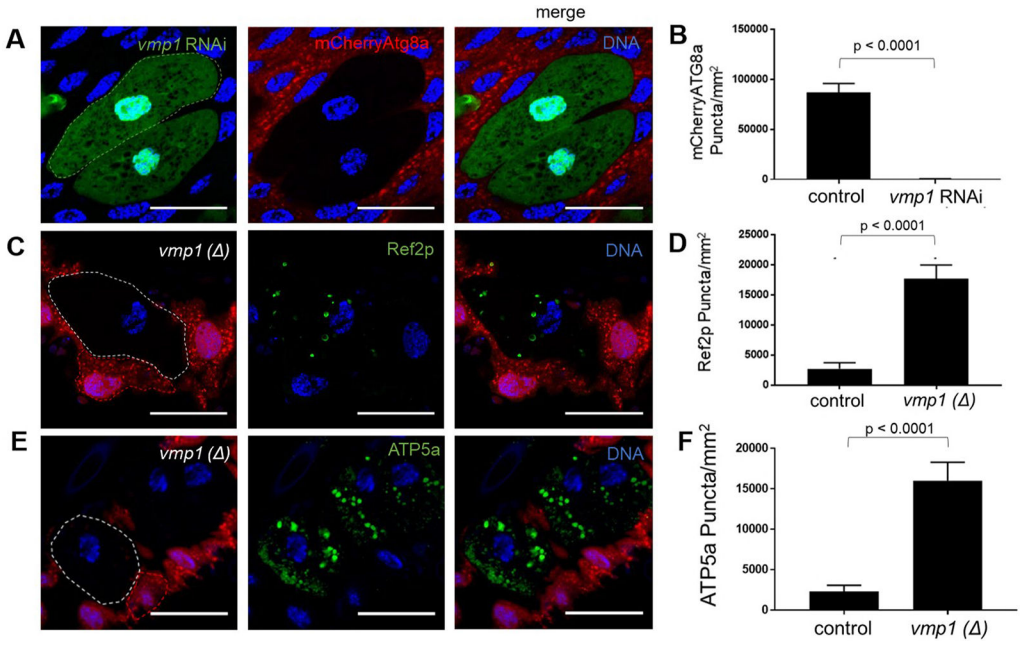

Figure 1. Vmp1 is required for autophagy in *Drosophila* intestines

(A) *vmp1* RNAi intestine cells (green) 2 hours after pupariation exhibit decreased mCherryAtg8a reporter puncta formation (red) compared to neighboring control cells (non-green). (B) Quantification of mCherryAtg8a puncta in *vmp1* RNAi cells (n=8) compared to control cells (n=16). (C) *vmp1(Δ)* mutant cells (non-red, white dotted line) possess increased Ref2p/p62 puncta (green) compared to neighboring control cells (red) in intestines 2 hours after pupariation. (D) Quantification of Ref2p puncta in *vmpl(Δ)* mutant (n=9) and control cells (n=8) 2 hours after pupariation. (E) *vmp1(Δ)* loss-of-function mutant cells (non-red, white dotted line) possess elevated mitochondrial ATP5a puncta (green) compared to neighboring control cells (red) in intestines 2 hours after pupariation. (F) Quantification of ATP5a puncta in *vmp1(Δ)* mutant (n=6) and control cells (n=16) 2 hours after pupariation. Scales bars in (A), (C) and (E) represent 40 μm. Error bars in (B), (D) and (F) are SEM. Thresholding in (A), (C), and (E) were based on maximizing the quality of signals without over-saturation. Representative of 3 or more independent biological experiments. See also Figure S1.

Author Manuscript Author Manuscript Author Manuscript Author Manuscript

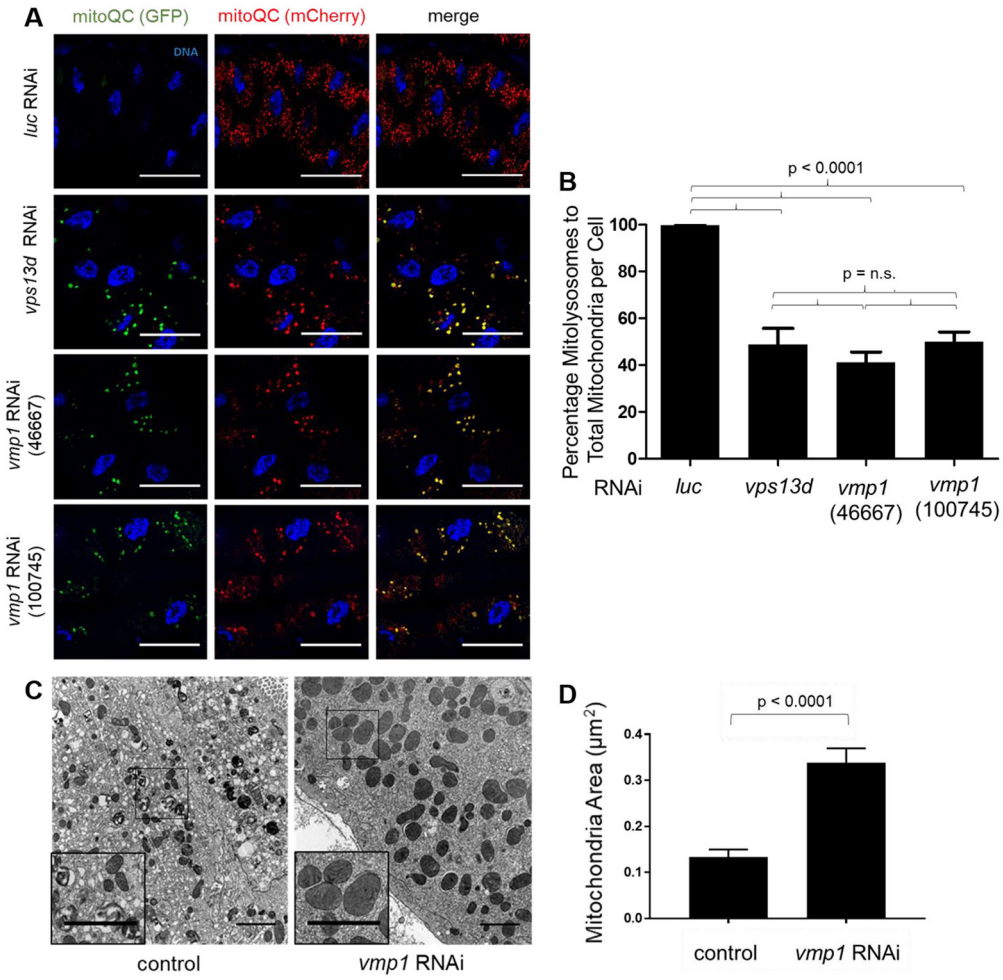

Figure 2. Vmp1 is required for mitophagy and normal mitochondrial morphology in *Drosophila* intestines

(A) Mito-QC expression was driven by intestine-specific NP1-GAL4 in different genotypes and analyzed in all intestine cells 2 hours after pupariation. Control *luciferase (luc)* RNAi-expressing cells possessed mostly red puncta (reflecting mitochondria in autolysosomes, mitolysosomes), while intestine cells expressing RNAi against either *vps13d* or 2 distinct *vmp1* RNAi expressing constructs (#46667 and #100745) all exhibited yellow puncta, reflecting mitochondria that failed to get cleared by mitophagy. (B) Quantification of the percentage of mitolysosomes to total mitochondria puncta in *luc* (n=10) RNAi-, *vps13d* (n=10) RNAi-, *vmp1* (#46667) (n=10) RNAi-, and *vmp1* (#100745) (n=8) RNAi-expressing cells 2 hours after pupariation. (C) TEM images of cells from intestines expressing either control *luciferase (luc)* RNAi or *vmp1* RNAi (#100745) 2 hours after pupariation. Enlarged regions are outlined by a black box. (D) Quantification of the size of mitochondria in either control *luc* (n=53) RNAi- or *vmp1* (n=51) RNAi-expressing intestine cells 2 hours after pupariation. Scales bars in (A) represent 40 μm. Scale bars in (C) represent 2.0 μm. Error bars in (B) and (D) are SEM. Thresholding in (A) was based on maximizing the quality of signal without over-saturation. Representative of 3 or more independent biological experiments. See also Figure S2.

Author Manuscript Author Manuscript Author Manuscript Author Manuscript

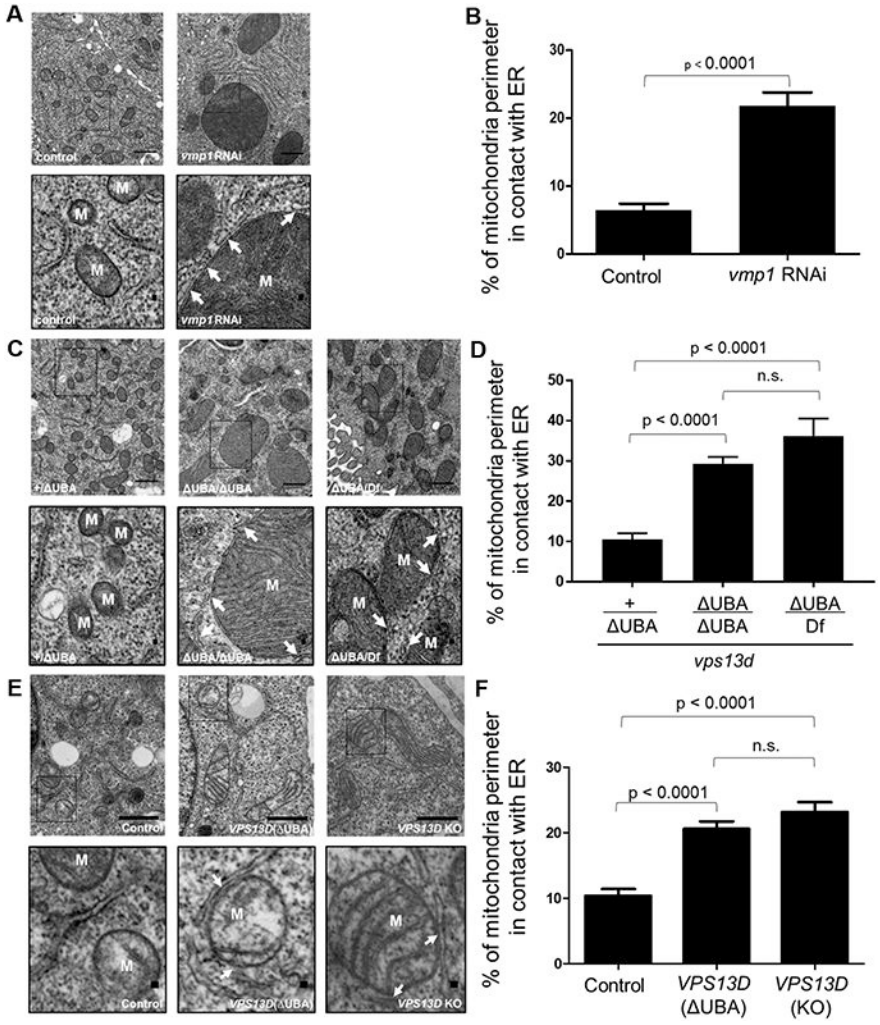

Figure 3. Vmp1 and Vps13D regulate mitochondria and ER contact.

(A) TEM images of cells from intestines expressing either control *luciferase (luc)* RNAi or *vmp1* RNAi (#100745) 2 hours after pupariation. Enlarged regions are outlined by a black box. Mitochondria (M) and ER (arrows) are indicated. (B) Quantification of the perimeter of mitochondria in contact with ER in either control *luc* (n=100) RNAi- or *vmp1* (n=78) RNAi-expressing intestine cells 2 hours after pupariation. Mitochondria and ER contact sites are defined as being separated by 0.03 μm or less and having a contact length of at least 0.02 μm *(16)*. (C) TEM images of cells from either control *+/vps13d (*ΔUBA), *vps13d (*ΔUBA)/*vps13d (*ΔUBA), or *vps13d (*ΔUBA)/*Df* intestines 2 hours after pupariation. (D) Quantification of mitochondria and ER contact in either control *+/vps13d (*ΔUBA) (n=50), *vps13d (*ΔUBA)/*vps13d (*ΔUBA) (n=50), or *vps13d (*ΔUBA)/*Df* (n=50) intestines 2 hours after pupariation. (E) TEM images of either wild-type control, *VPS13D (*ΔUBA), or *VPS13D* KO (exon 3 deletion) HeLa cells. (F) Quantification of mitochondria and ER contact in either control (n=96), *VPS13D (*ΔUBA) (n=116), or *VPS13D* KO (exon 3 deletion) (n=100) HeLa cells. In (A), (C), and (E), arrows represent regions of contact between mitochondria (M) and ER. Scale bars in top panels represent 0.5 μm and bottom

panels represent 0.03 μm. Error bars in (B), (D), and (F) are SEM. Representative of 3 or more independent biological experiments. See also Figure S3.

Author Manuscript Author Manuscript Author Manuscript Author Manuscript

Author Manuscript Author Manuscript Author Manuscript Author Manuscript

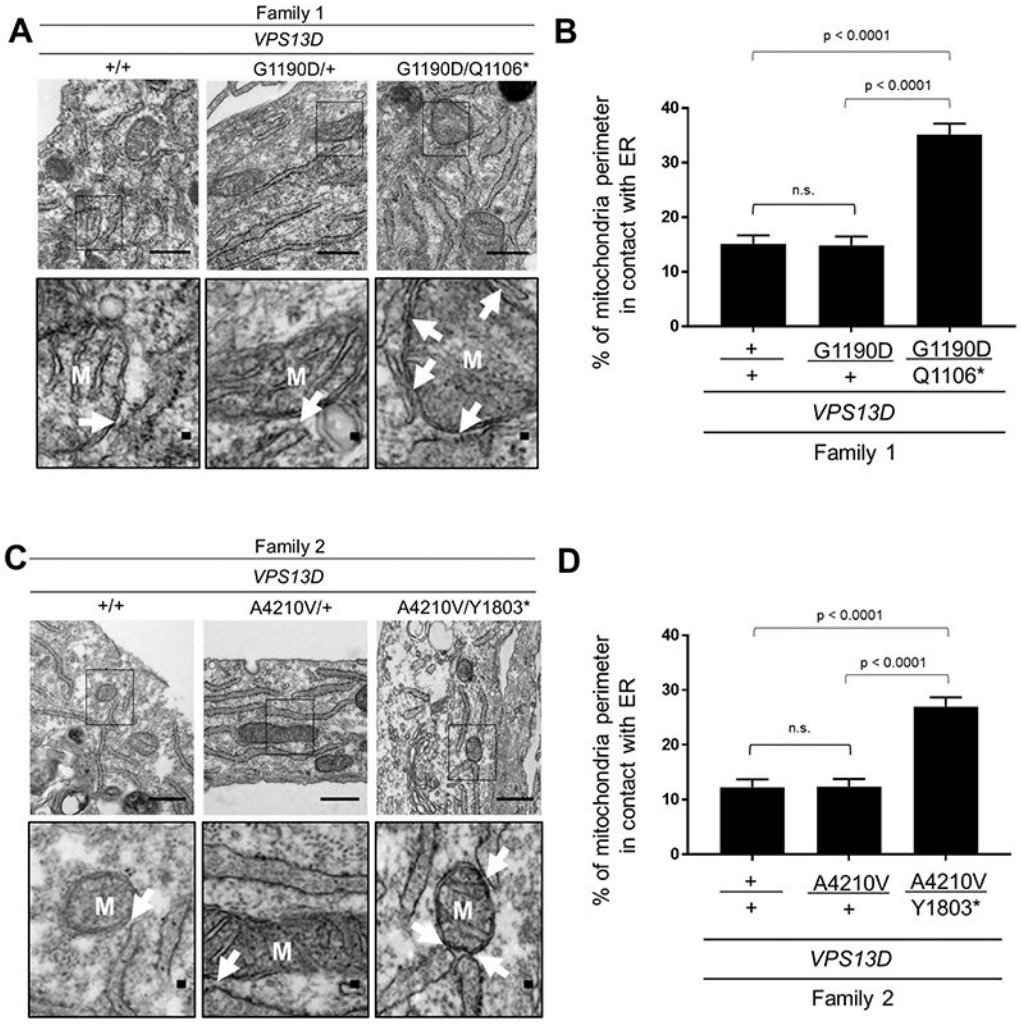

Figure 4. Fibroblasts derived from patients with neurological symptoms associated with *VPS13D* mutations have increased mitochondria and ER contact

(A) TEM images of fibroblast cells derived from a family with mutations in *VPS13D* (Family 1). Cells were derived from either an unrelated donor without mutations in *VPS13D* (+/+), a relative carrying the G1190D allele for *VPS13D* (G1190D/+), or a patient with neurological symptoms carrying the G1190D and Q1106* mutations in *VPS13D* (G1190D/Q1106*). Enlarged regions are outlined by a black box, mitochondria (M) and ER (arrows) are indicated. (B) Quantification of mitochondria and ER contact in *VPS13D* (+/+) (n=54), (G1190D/+) (n=50), and (G1190D/Q1106*) (n=50) fibroblasts derived from Family 1. (C) TEM images of fibroblast cells derived from a family with mutations in *VPS13D* (Family 2). Cells were derived from either an unrelated donor without mutations in *VPS13D* (+/+), a relative carrying the A4210V allele for *VPS13D* (A4210V/+), or the patient with neurological symptoms carrying the A4210V and Y1803* mutations in *VPS13D* (A4210V and Y1803*). (D) Quantification of mitochondria and ER contact in *VPS13D* (+/+) (n=50), (A4210V/+) (n=56), and (A4210V/Y1803*) (n=50) fibroblasts derived from Family 2. In (A) and (C), scale bars in top panels are 0.5 μm and in bottom panels are 0.03 μm. Error bars

in (B) and (D) are SEM. Representative of 3 or more independent biological experiments. See also Figure S4.

Author Manuscript Author Manuscript Author Manuscript Author Manuscript

Author Manuscript Author Manuscript Author Manuscript Author Manuscript

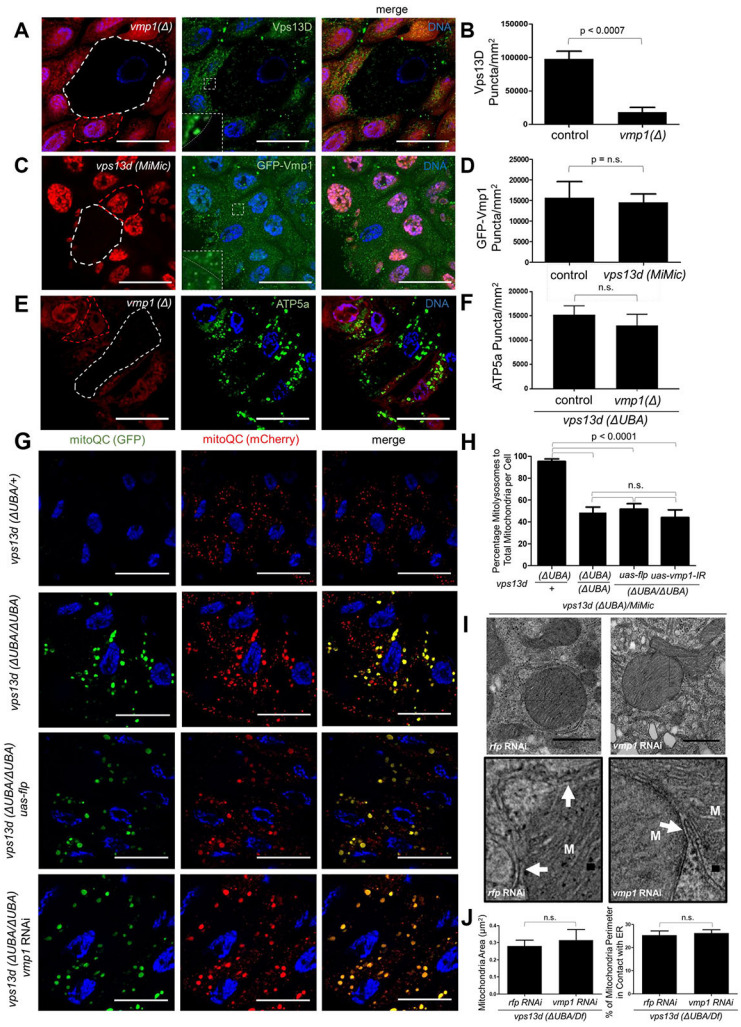

Figure 5. Vps13d and Vmp1 function in a pathway to regulate mitophagy and mitochondrial morphology

(A) *vmp1 (Δ)* loss-of-function mutant cells (non-red, white dotted line) possess fewer Vps13D puncta (green) compared to neighboring control cells (red) in intestines 2 hours after pupariation. (B) Quantification of Vps13D puncta in *vmp1(Δ)* mutant (n=6) and control (n=16) intestine cells 2 hours after pupariation. (C) *vps13d (MiMic)* mutant cells (lacking nuclear RFP, white dotted line) do not have altered GFP-Vmp1 in larval intestines 2 hours after pupariation. Antibody against GFP was used to enhance GFP-Vmp1 signal. (D) Quantification of GFP-Vmp1 puncta in *vps13d (MiMic)* mutant (n=8) and control (n=14) intestine cells 2 hours after pupariation. (E) *vmp1*(Δ) and *vps13d (ΔUBA)* double mutant cells (non-red, white dotted line) exhibit similar levels of mitochondrial ATP5a protein compared to neighboring control *vmp1(Δ)/+* and *vps13d (ΔUBA)* single mutant cells (red) 2 hours after pupariation. (F) Quantification of ATP5a puncta in *vmp1*(Δ) and *vps13d (ΔUBA)* double mutant (n=8) and *vmp1(Δ)/+* and *vps13d (ΔUBA)* single mutant (n=14) control intestine cells 2 hours after pupariation. (G) Mito-QC expression was driven by intestine-specific NP1-GAL4 in different genotypes and analyzed in intestine cells 2 hours after pupariation. Control *vps13d (ΔUBA)/+* cells possessed mostly red puncta (reflecting

Author Manuscript Author Manuscript Author Manuscript Author Manuscript

mitochondria in autolysomes, mitolysosomes), while *vps13d (ΔUBA/ΔUBA)* homozygous mutant, *vps13d (ΔUBA/ΔUBA)* mutant expressing *flp*, and *vps13d (ΔUBA/ΔUBA)* mutant with *vmp1* RNAi-expressing intestine cells all exhibited large yellow puncta (reflecting mitochondria that fail to be cleared by mitophagy). (H) Quantification of the percentage of mitolysosomes to total mitochondria puncta in *vps13d (ΔUBA)/+* (n=10), *vps13d (ΔUBA/ΔUBA)* (n=10), *vps13d (ΔUBA/ΔUBA), UAS-flp* (n=11), and *vps13d (ΔUBA/ΔUBA), vmp1* RNAi (100745) (n=10), cells 2 hours after pupariation. (I) TEM images of cells from either control *vps13d (ΔUBA)/MiMic* expressing *rfp* RNAi or *vps13d (ΔUBA)/MiMic* expressing *vmp1* RNAi intestines 2 hours after pupariation. Insets in (A) and (C) represent enlarged regions, with dashed lines inside representing cell borders. Enlarged regions in (I) are outlined by a black box, mitochondria (M) and ER (arrows) are indicated. (J) Quantification of either mitochondrial size or mitochondria and ER contact in either control *vps13d (ΔUBA)/MiMic* expressing *rfp* RNAi (n=55) or *vps13d (ΔUBA)/MiMic* expressing *vmp1* RNAi (#100745) (n=62) intestine cells 2 hours after pupariation. Scale bars in (A), (C), (E), and (G) are 40 μm. Scale bars in top panel of (I) represent 0.5 μm while scale bars in bottom panels represent 0.03μm. Error bars in (B), (D), and (F), (H), and (J) are SEM. Thresholding in (A), (C), (E) and (G) were based on maximizing the quality of signals without over-saturation. Representative of 3 or more independent biological experiments. See also Figure S5.

Author Manuscript Author Manuscript Author Manuscript Author Manuscript

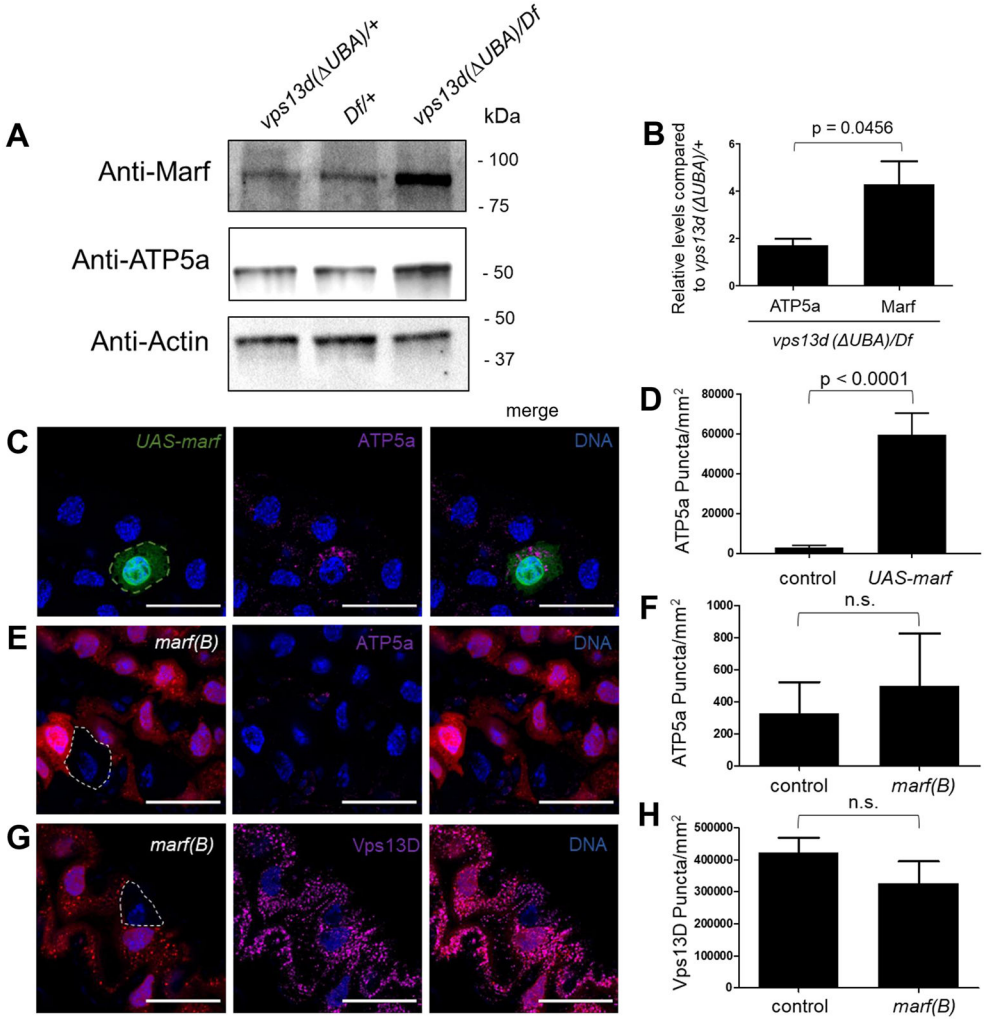

Figure 6. Vps13d functions upstream of Marf to mediate mitochondrial clearance.

(A) Western blot of lysates from *vps13d(ΔUBA)/+, Df/+*, and *vps13d(ΔUBA)/Df* intestines 2 hours after pupariation that was probed with antibodies against Marf, ATP5a and Actin. (B) Quantification of relative levels of Marf and ATP5a in *vps13d(ΔUBA)/+, Df/+*, and *vps13d(ΔUBA)/Df* intestines 2 hours after pupariation compared to Actin. (C) Intestine cells that overexpress *marf* using the Act-GAL4 (green) were stained with antibodies against ATP5a (purple) and compared to neighboring control cells (non-green). (D) Quantification of levels of ATP5a puncta in *marf* overexpressing intestine cells 2 hours after pupariation compared to control cells. (E) Intestines 2 hours after pupariation containing *marf(B)* loss-of-function mutant cells (non-RFP) were stained with antibody against ATP5a (purple). (F) Quantification of levels of ATP5a puncta in *marf(B)* loss-of-function mutant cells (n=6) 2 hours after pupariation compared to control cells (n=14). (G) Intestines 2 hours after pupariation containing *marf(B)* loss-of-function mutant cells (non-RFP) were stained with antibody against Vps13D (purple). (H) Quantification of levels of Vps13D puncta in *marf(B)* loss-of-function mutant cells (n=6) 2 hours after pupariation compared to control cells (n=13). Scale bars in (C), (E), and (G) represents 40 μm. Error bars in (B), (D), (F), and (H) are SEM. Thresholding in (C), (E), and (G) were based on maximizing the quality of

signals without over-saturation. Representative of 3 or more independent biological experiments. See also Figure S6.

Author Manuscript Author Manuscript Author Manuscript Author Manuscript

Author Manuscript Author Manuscript Author Manuscript Author Manuscript

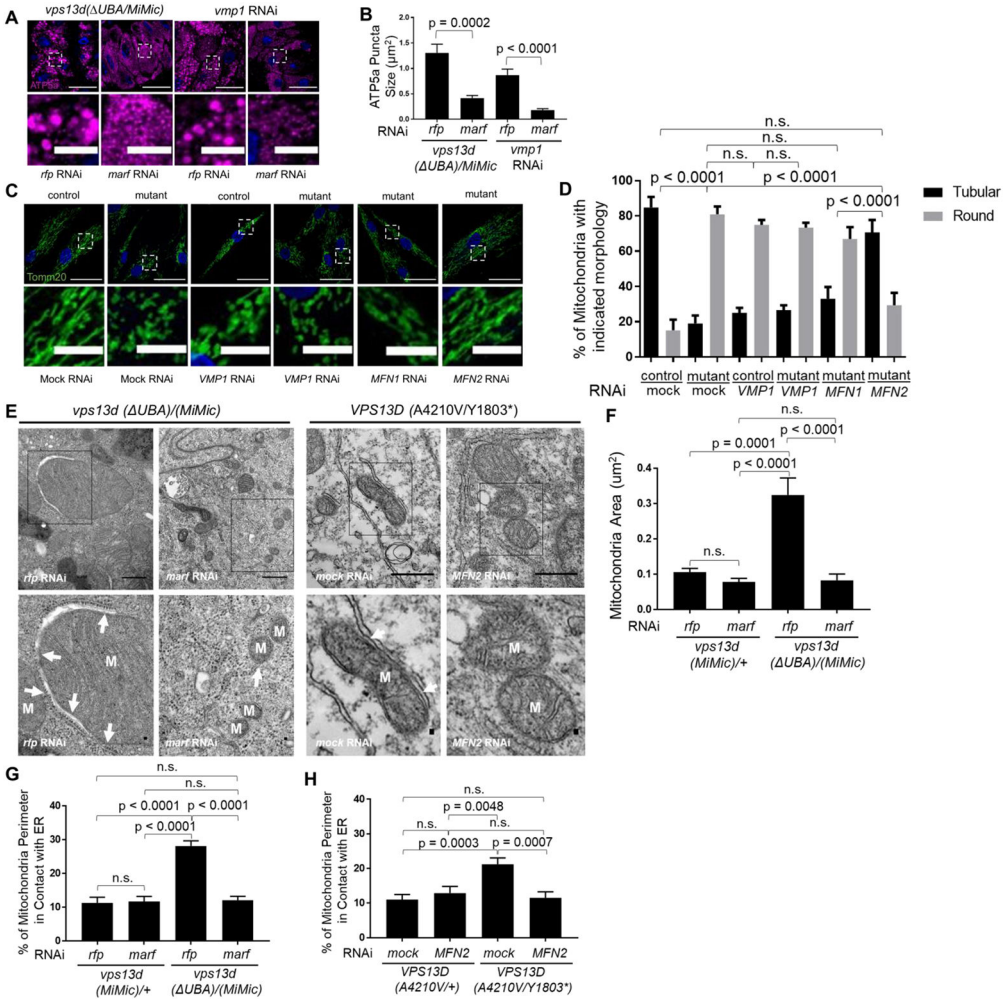

Figure 7. Reduction of Marf/Mfn2 function suppresses Vps13D and Vmp1 phenotypes

(A) *vps13d (ΔUBA/MiMic)* and *vmp1* RNAi-expressing intestines 2 hours after pupariation were stained with antibody against ATP5a (purple) with control *rfp* RNAi or *marf* RNAi expression. (B) Quantification of ATP5a puncta size in *vps13d (ΔUBA/MiMic)* and *vmp1* RNAi-expressing intestines 2 hours after pupariation with control *rfp* RNAi (n=13 for *vps13d*, n=11 for *vmp1*) or *marf* RNAi (n=12 for *vps13d* and *vmp1*) expression. (C) Fibroblasts from a patient (mutant) with transheterozygous *VPS13D* mutations (G1190D/Q1106*) were stained with TOMM20 antibody (green) and compared to heterozygous control (G1190D/+) fibroblasts (control). Control fibroblasts were transfected with negative control mock and *VMP1* RNAi and mutant fibroblasts were transfected with mock, *MFN2* and *VMP1* RNAi. (D) Quantification of mitochondria morphology in control fibroblasts transfected with mock RNAi (n=11) and *VMP1* RNAi (n=10) compared to mutant fibroblasts transfected with mock RNAi (n=11), *VMP1* RNAi (n=15), and *MFN2* RNAi (n=14). (E) Representative TEM images of cells from *vps13d (*ΔUBA)/*(MiMic)* intestine cells expressing either *rfp* (control) or *marf* RNAi (left panels) 2 hours after pupariation, and *VPS13D (A4210V/Y1803*)* patient fibroblasts treated with either negative control mock or *MFN2* RNAi (right panels). Enlarged regions are outlined by a black box, mitochondria (M) and ER (arrows) are indicated. (F) Quantification of mitochondrial size in *vps13d (MiMic)/+*

Author Manuscript Author Manuscript Author Manuscript Author Manuscript

(n=62) intestine cell expressing *rfp* RNAi, *vps13d (MiMic)/+* (n=82) intestine cells expressing *marf* RNAi, *vps13d (*ΔUBA)/*(MiMic)* (n=84) intestine cell expressing *rfp* RNAi, and *vps13d (*ΔUBA)/*(MiMc)* (n=72) intestine cells expressing *marf* RNAi 2 hours after pupariation. (G) Quantification mitochondria and ER contact in *vps13d (MiMic)/+* (n=62) intestine cells expressing *rfp* RNAi, *vps13d (MiMic)/+* (n=82) intestine cells expressing *marf* RNAi, vps13d (ΔUBA)/(*MiMic)* (n=84) intestine cells expressing *rfp* RNAi, and *vps13d (*ΔUBA)/(*MiMic)* (n=72) intestine cells expressing *marf* RNAi 2 hours after pupariation. (H) Quantification of mitochondria and ER contact in *VPS13D (A4210/+)* heterozygous control fibroblasts treated with mock (n=50) and *MFN2* (n=51) RNAi compared to *VPS13D (A4210V/Y1803*)* mutant fibroblasts treated with mock (n=50) and *MFN2* (n=50) RNAi. Scale bar in top panels of A) and C) represents 40 μm, bottom panels represent 10μm. Scale bars in the upper panels of (E) represent 0.5 μm while scale bars in bottom panels represent 0.03μm. Error bars in (B), (D), (F), (G), and (H) are SEM. Thresholding in (A) and (C) were based on maximizing the quality of signals without over-saturation. Representative of 3 or more independent biological experiments. See also Figure S7.

Author Manuscript Author Manuscript Author Manuscript Author Manuscript

KEY RESOURCES TABLE

REAGENT or RESOURCE	SOURCE	IDENTIFIER
Antibodies		
Vps13D	Eric Baehrecke	[7]
ref(2)p	Gabor Juhasz	[46]
ATP synthase complex V	Abcam	Ab14748
GFP	Abcam	ab13970
SERCA	Mani Ramaswami	[47]
Actin	Proteintech	60008-1-Ig
TOMM20	Abcam	ab78547
Marf	Alexander Whitworth	[31]
COX IV	Abcam	ab14744
FLAG	Abcam	Ab1162
FLAG M2	Millipore Sigma	F1804
MFN2	Abnova	H00009927-M03
MFN1	Proteintech	13798-1-AP
anti-mouse AlexaFluor 647	Invitrogen	A-21235
anti-rabbit Alexafluor 546	Invitrogen	A-11035
anti-chicken AlexaFluor 488	Invitrogen	A-11039
anti-mouse Alexa Fluor 488	Invitrogen	A-11029
Oregon Green 488 goat anti-rabbit	Molecular Probes	O-6381
Bacterial and Virus Strains		
E. coli/One Shot TOP10	Invitrogen	C404010
Chemicals, Peptides, and Recombinant Proteins		
Fetal bovine serum	Gemini Bio Products	100-106
DMEM	Life Technologies	31053-028
Penicillin-streptomycin	GIBCO	15140122
PBS	GIBCO	70011
25% Glutaraldehyde	Electron Microscopy Sciences	16220
Sodium cacodylate	Electron Microscopy Sciences	11650
osmium tetroxide	SPI	2601
propylene oxide	SPI	75-56-9
SPI-pon/Araldite 6005 epoxy embedding kit	SPI	02635-AB
Paraformaldehyde	Electron Microscopy Sciences	15710
Dimethyl sulfoxide	Sigma	D2438
Triton x-100	Sigma	T8787
Vectashield	Vector Laboratories	H-1200
Tris-HCl	Sigma	T3253
NaCl	Fisher	BP358-212

Author Manuscript Author Manuscript Author Manuscript Author Manuscript

REAGENT or RESOURCE	SOURCE	IDENTIFIER
Goat serum	Sigma	G9023
EDTA	Quality Biological	351-027-101
3xFLAG peptide	Sigma	F4799-4MG
Carbonyl cyanide 4-(trifluoromethoxy)phenylhydrazone (FCCP)	Sigma	C2920
Antimycin A from Streptomyces sp.	Sigma	A8674
Oligomycin A	Sigma	75351
Critical Commercial Assays		
Deposited Data		
Project Achiles	Broad Institute	[48][49]
Experimental Models: Cell Lines		
HeLa	ATCC	CCL-2
HeLa *VPS13D* ΔUBA deletion (ΔUBA)	Eric Baehrecke	[7]
HeLa *VPS13D* exon 3 deletion (KO #45)	Eric Baehrecke	[7]
Family 1 Patient Fibroblasts (G1190D/Q1106*): UM1.2	Margit Burmeister	[10]
Family 1 Heterozygote Fibroblasts (Q1106*/+): UM1.17	Margit Burmeister	[10]
Family 1 Unrelated Fibroblasts (+/+): UMCtrl1	Margit Burmeister	[10]
Family 2 Patient Fibroblasts (A4210V/Y1803*): LUB1.1	Katja Lohmann	[10]
Family 2 Heterozygote Fibroblasts (Y1803*/+): LUB1.3	Katja Lohmann	[10]
Family 2 Unrelated Fibroblasts (+/+): LUBCtrl1	Katja Lohmann	[10]
Experimental Models: Organisms/Strains		
Drosophila melanogaster/ w^{1118}	Bloomington *Drosophila* stock center	5905
Drosophila melanogaster/y^1 w^{1118} hsFlp; If/CyO; Act>CD2>GAL4, UAS–nlsGFP/TM6B	Eric Baehrecke	N/A
Drosophila melanogaster/y^1 w^{1118} hsFlp; pmCherry–Atg8a; Act>CD2>GAL4, UAS–nlsGFP/TM6B	Eric Baehrecke	N/A
Drosophila melanogaster/w^{1118}; P{GD15932}v46667	VDRC	46667
Drosophila melanogaster/w^{1118}; P{KK108366}VIE-260B	VDRC	100745
Drosophila melanogaster/w^{1118}; P{KK105681}VIE-260B	VDRC	105261
Drosophila melanogaster/w^{1118}; P{KK105681}VIE-260B; P{GD15932}v46667	Eric Baehrecke	N/A
Drosophila melanogaster/ y^1 sc* v^1 sev21; P{TRiP.HMS01784}attP2	Bloomington *Drosophila* stock center	38320
Drosophila melanogaster/ y^1 v^1; P{TRiP.JF01355}attP2	Bloomington *Drosophila* stock center	31603
Drosophila melanogaster/ y^1 sc* v^1 sev^{21}; P{TRiP.HMS05713}attP40	Bloomington *Drosophila* stock center	67852
Drosophila melanogaster/ y^1 sc* v^1 sev^{21}; P{TRiP.HMS05713}attP40; Mi{MIC}Vps13DMI11101/TM6B	Eric Baehrecke	N/A
Drosophila melanogaster/ y^1 w*; Mi{MIC}Vps13DMI11101/TM6B	Bloomington *Drosophila* stock center	56282
Drosophila melanogaster/ w^{1118}; Df(3L)BSC631/TM6C, cu^1 Sb^1	Bloomington *Drosophila* stock center	25722
Drosophila melanogaster/ w^{1118}; Df(3L)BSC631/TM6B	Eric Baehrecke	N/A

Author Manuscript Author Manuscript Author Manuscript Author Manuscript

REAGENT or RESOURCE	SOURCE	IDENTIFIER
Drosophila melanogaster/w^{1118}; Dp(1;3)RC025, PBac{RC025}VK00033/TM6C, Sb1	Bloomington *Drosophila* stock center	38486
Drosophila melanogaster/ w^{1118}; P{20XUAS-tdTomato-Sec61β}attP2	Bloomington *Drosophila* stock center	64747
Drosophila melanogaster/ y^{1} w*; P{Act5C-GAL4}25FO1/CyO, y+	Bloomington *Drosophila* stock center	4414
Drosophila melanogaster/ y^{1} w* MarfB P{neoFRT}19A/FM7c, P{GAL4-Kr.C}DC1, P{UAS-GFP.S65T}DC5, sn+	Bloomington *Drosophila* stock center	67154
Drosophila melanogaster/y^{1} w*; P{UAS-Marf.HA.S}3/T(2;3)TSTL, CyO: TM6B, Tb1	Bloomington *Drosophila* stock center	67157
Drosophila melanogaster/w*; P{GawB}Myo31DFNP0001, P{UAS-mito-HA-GFP.AP}2/CyO	Eric Baehrecke	N/A
Drosophila melanogaster/w*; P{w[+mW.hs]=FRT(w[hs])}2A	Bloomington *Drosophila* stock center	1997
Drosophila melanogaster/ w^{1118}; P{Ubi-GFP.nls}3L1 P{Ubi-GFP.nls}3L2 P{FRT(whs)}2A	Bloomington *Drosophila* stock center	5825
Drosophila melanogaster/ P{hsFLP}12, w^{1118}; P{Ubi-GFP.nls}3L1 P{Ubi-GFP.nls}3L2 P{FRT(whs)}2A	Eric Baehrecke	N/A
Drosophila melanogaster/ P{Ubi-mRFP.nls}1, w^{1118}, P{neoFRT}19A, P{hsFLP}12	Eric Baehrecke	N/A
Drosophila melanogaster/w*; P{w[+mC]=Ubi-GFP.D}61EF, P{w[+mW.hs]=FRT(w[hs])}2A	Bloomington *Drosophila* stock center	1626
Drosophila melanogaster/ w^{1118};; P{w[+mW.hs]=FRT(w[hs])}2A, Mi{MIC}Vps13DMI11101/TM6B	Eric Baehrecke	[7]
Drosophila melanogaster/w*; P{w[+mC]=UAS-FLP.D}JD2	Bloomington *Drosophila* stock center	4540
Drosophila melanogaster/w*; P{GawB}Myo31DFNP0001 / CyO, P{UAS-lacZ.UW14}UW14	*Drosophila* Genetic Resource Center	112001
Drosophila melanogaster/w*; P{GawB}Myo31DFNP0001; *vps13d (ΔUBA)/TM6B*	Eric Baehrecke	N/A
Drosophila melanogaster/ P{UAS-mito-QC}attP16	Alexander J. Whitworth	[5]
Drosophila melanogaster/ P{UAS-mito-QC}attP16, P{GawB}Myo31DFNP0001	Eric Baehrecke	N/A
Drosophila melanogaster/ P{UAS-mito-QC}attP16, P{GawB}Myo31DFNP0001; *vps13d (ΔUBA)/TM6B-GFP*	Eric Baehrecke	N/A
Drosophila melanogaster/ w^{1118}; P{UAS-mito-HA-GFP.AP}2/CyO	Bloomington *Drosophila* stock center	8442
Drosophila melanogaster/ *vps13d (ΔUBA)/TM6B*	Eric Baehrecke	[7]
Drosophila melanogaster/w*; P{w[+mC]=UAS-FLP.D}JD2; *vps13d (ΔUBA)/TM6B*	Eric Baehrecke	N/A
Drosophila melanogaster/w*; P{KK108366}VIE-260B; *vps13d (ΔUBA)/TM6B*	Eric Baehrecke	N/A
Drosophila melanogaster/w*; P{KK108366}VIE-260B; Mi{MIC}Vps13DMI11101/TM6B*)/TM6B*	Eric Baehrecke	N/A
Drosophila melanogaster/w*; P{KK108366}VIE-260B; {w[+mW.hs]=FRT(w[hs])}2A, Mi{MIC}Vps13DMI11101/TM6B	Eric Baehrecke	N/A
Drosophila melanogaster/ P{Ubi-mRFP.nls}1, w^{1118}, P{neoFRT}19A, P{hsFLP}12;; *vps13d (ΔUBA)/TM6B*	Eric Baehrecke	N/A
Drosophila melanogaster/ w^{1118}, *vmp1(Δ)*	This paper	N/A
Drosophila melanogaster/ w^{1118}, P{neoFRT}19A, *vmp1(Δ)*	This paper	N/A

Author Manuscript Author Manuscript Author Manuscript Author Manuscript

REAGENT or RESOURCE	SOURCE	IDENTIFIER
Drosophila melanogaster/ w^{1118}, P{neoFRT}19A, *vmp1(Δ);; vps13d (ΔUBA)/ TM6B*	This paper	N/A
Drosophila melanogaster/ w^{1118}, *gfp-vmp1*	This paper	N/A
Drosophila melanogaster/ w^{1118}, *gfp-vmp1*;; P{w[+mW.hs]=FRT(w[hs])}2A, Mi{MIC}Vps13DMI11101/TM6B	This paper	N/A
Drosophila melanogaster/ w^{1118}, *gfp-vmp1;* P{GawB}Myo31DFNP0001	This paper	N/A
Drosophila melanogaster/ P{hsFLP}12;; P{Ubi-mRFP.nls}3L, P{w[+mW.hs]=FRT(w[hs])}2A	Eric Baehrecke	N/A
Drosophila melanogaster/ P{hsFLP}12; P{GawB}Myo31DFNP0001; P{Ubi-mRFP.nls}3L, P{w[+mW.hs]=FRT(w[hs])}2A	Eric Baehrecke	N/A
Drosophila melanogaster/w^{1118}; P{KK105681}VIE-260B; Mi{MIC}Vps13DMI11101/TM6B	Eric Baehrecke	N/A
Drosophila melanogaster/w^{1118};; *vps13d-3xFLAG*	This paper	N/A
Oligonucleotides		
Primer to design sgRNA1: TGTTGTTGTGACGATTGCTC	Integrated DNA Technologies	N/A
Primer to design sgRNA2: TTACGGGACTAGAAAATCAG	Integrated DNA Technologies	N/A
Primer to design sgRNA3: TGCTGTGACATTTAAGCGGT	Integrated DNA Technologies	N/A
Primer to design sgRNA4: CGAATGCTGTGACATTTAAG	Integrated DNA Technologies	N/A
Single-stranded donor DNA to design *vmp1(Δ)*: CAAAAACCGTGAAAAACACAGCCGCTTGCAAGCCAACCGCTTAAATGTC ACAGCATTCGAAAAAGGAAACCACCAGCAGCAGCGGTAGCCATGCGGCC CAAAAATCAGTGGATCAGTCTTCTGTTGATCTTTTTCCCCAACCCTTGGT TTTCGTTTAAATTATTTTGTATATTGCGGCTTTCGCTCTTAGTCAAATGATG	Integrated DNA Technologies	N/A
Primer to screen and verify 5' of *vmp1(Δ)* and *gfp-vmp1*: CTTTTCGAATCGCCGGCATTTACATCAC	Integrated DNA Technologies	N/A
Primer to screen and verify 3' of *vmp1(Δ)* and *gfp-vmp1*: CATCATTTGACTAAGAGCGAAAGCCGC	Integrated DNA Technologies	N/A
Primer to verify 3' N terminus *vmp1* of *gfp-vmp1*: CTGATGCTGTTGCTATTGCCGTTTCC	Integrated DNA Technologies	N/A
siRNA NC negative (mock) control: UUCUCCGAACGUGUCACGUTT	Hong Zhang	[22]
siRNA Human *VMP1*: 5'-GGAAUGGACCUCAAAAUUATT-3'	Hong Zhang	[22]
siRNA SMARTpool for Human *MFN2*: GACUAUAAGCUGCGAAUUA CAUGAGGCCUUUCUCCUUA GCAACUCUAUCGUCACAGU GGUGGACGAUUACCAGAUG	Dharmacon	N/A
siRNA SMARTpool for Human *MFN1:* CGAUGAAGUAAACGCCUUA CAUGAUAGGAGGAAACGAA CAGAAUAUAUGGAAGACGU GGAAGUUCUUAGUGCUAGA	Dharmacon	N/A
Recombinant DNA		
Plasmid: U6droBsagRNA	Drosophila Genomics Resource Center	1341
Plasmid: pCR™2.1-TOPO® vector	Thermo Fisher Scientific	K450002
Software and Algorithms		
ImageJ	NIH	https://imagej.nih.gov/ij/

REAGENT or RESOURCE	SOURCE	IDENTIFIER
Zen Black	Zeiss	N/A
Prism	Graphpad Software, Inc.	https://www.graphpad.com/scientific-software/prism/
Biorender	Biorender	https://biorender.com/
Other		

Author Manuscript Author Manuscript Author Manuscript Author Manuscript